s-Block Complexes of iso-Tellurazole *N*-Oxides

A STUDY OF THE COORDINATION CHEMISTRY OF ISO-TELLURAZOLE N-OXIDES WITH *s*-BLOCK ELEMENTS

BY
JIN ZHAO WANG B.SC.

A THESIS

SUBMITTED TO THE SCHOOL OF GRADUATE STUDIES

IN PARTIAL FULFILLMENT OF THE REQUIREMENTS

FOR THE MASTER'S DEGREE

MCMASTER UNIVERSITY

McMaster University MASTER of SCIENCE (2021)

Hamilton, Ontario (Chemistry)

TITLE: A Study of the Coordination Chemistry of Iso-Tellurazole *N*-Oxides with s-block elements

AUTHOR: JinZhao Wang

SUPERVISOR: Associate Professor Ignacio Vargas-Baca

NUMBER OF PAGES: pages i-xiii, pages 55.

Abstract

The study of the macrocyclic aggregates of iso-tellurazole *N*-oxide has previously unveiled a wide variety of complexes with transition metal ions. The compound 3-methyl-5-phenyl-1,2-tellurazole-2-oxide and its derivatives bind soft d^6, d^8 and d^{10} metal ions exclusively by tellurium. The electron withdrawing ability of the cations strengthen the Te···O chalcogen bonding (ChB) interactions.

In this thesis, we investigated the coordination chemistry of iso-tellurazole *N*-oxide with hard metal ions from elements of groups 1 and 2, as salts with weakly-coordinating anions. X-ray crystallography of the isolated products showed that the oxophilic nature of these cations results in coordination to the oxygen atom. However, formation of Te···O ChBs is not inhibited, in contrast to the cases in which oxygen binds protons or boranes.

Novel dodecameric macrocycles were obtained from experiments with Na^+ cations. The large supramolecular ring folds onto itself forming a cage-like structure capable of hosting molecules such as dioxane, THF and pyrazine. Their encapsulation is facilitated by the coordination to the metal ion. In the absence of such molecular guests, a tris-tetramer structure was assembled with four sodium ions. Although full refinement of its crystal structure is yet to be completed, the tris-tetramer suggests a mechanism that leads to the formation of the dodecamers. In contrast to Na^+, K^+ yielded a 1-D coordination polymer of the tetramers. The more oxophilic Mg^{2+} yielded complexes of macrocyclic hexamers of iso-tellurazole oxides linked by C-Te···O ChBs.

Acknowledgements

I thank my supervisor, Dr. Ignacio Vargas-Baca for being an extremely supportive supervisor, whom I think is both very knowledgeable and passionate towards chemistry.

I express my gratitude towards my supervisory committee member, Dr. David Emslie for his helpful suggestions and his generous supply of the $KBArF_{20}$ salt for my research.

I thank the NMR spectroscopy facility (Drs. Hilary Jenkins, Bob Berno), mass spectrometry facility, and the X-ray diffraction facility (Dr. Jim Britten).

I thank my funding sources: McMaster University, the Department of Chemistry & Chemical Biology, the Natural Science Engineering Research Council of Canada (NSERC), and the Ontario Graduate Scholarship (OGS).

I thank the staff and facilities of the Shard Hierarchical Academic Research Computing Network (SHARCNET: www.sharcnet.ca) as well as their support for licensing the DFT software used in this project.

I thank both past & present lab member and summer/undergraduate thesis students (Peter Ho, Justin Lomax, Yasmeen Shamiya, MaoHeng Wu, Matthew Craig, and Phillip MacDougall).

I also thank my family members for their constant support.

Table of Content

List of Figures

List of Schemes

List of Tables

List of Abbreviations and Symbols

δ	chemical shift, ppm (parts per million)
Å	Angstrom (1Å = 10^{-10} m)
a, b, c, α, β, γ	unit cell parameters (in crystallography)
ADF	Amsterdam Density Functional (software)
$BArF_{20}^-$	Tetrakis(pentafluorophenyl)borate
$BArF_{24}^-$	Tetrakis(3,5-bis(trifluoromethyl)phenyl)borate
ChB	Chalcogen bonding or chalcogen bond
cm^{-1}	Wavenumber
CSD	Cambridge Structural Database
DFT	Density functional theory
EA	Elemental analysis
Et	Ethyl, functional group
h	Plank's constant
K	Kelvin
k_B	Boltzmann's constant
G	Gibbs free energy
GGA	Generalized gradient approximation
GUI	Graphical user interface
H	Enthalpy
Me	Methyl, functional group
MS	Mass Spectrometry
Mp	Melting point
N_A	Avogadro's number
NMR	nuclear magnetic resonance (spectroscopy)
Ph	Phenyl, functional group
ppm	Parts per million
T	temperature
^{t}Bu	Tert-butyl, functional group
r_{vdW}	van der Waals radii
S	Entropy
SBI	secondary bonding interaction
U	Total internal energy
UV-Vis	ultraviolet-visible (spectroscopy)
THF	Tetrahydrofuran
VT	variable temperature (in NMR)
wR_2	weighted residual factor (in crystallography)
^{t}Bu	tert-butyl functional group
TZ2P	triple-ζ with two polarization function (basis set)

List of compounds

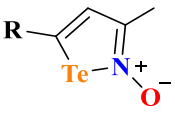

1a: R=Ph
1b: R=3,5-(^{t}Bu)$_2$C$_6$H$_3$
1c: R=H

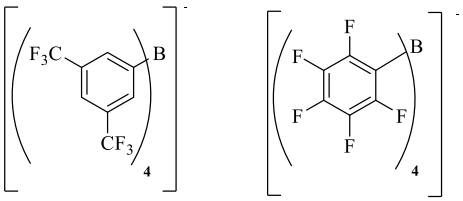

2a $[BArF_{24}]^-$
2b $[BArF_{20}]^-$

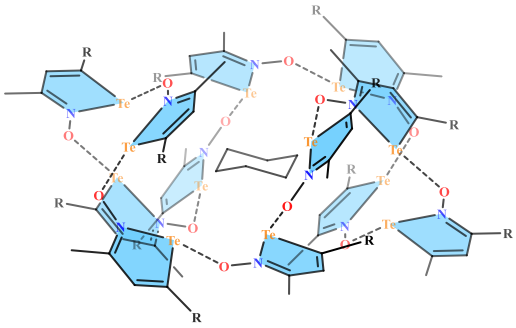

3
$C_6H_{12}\subset\{\mathbf{1a}_{12}\}$

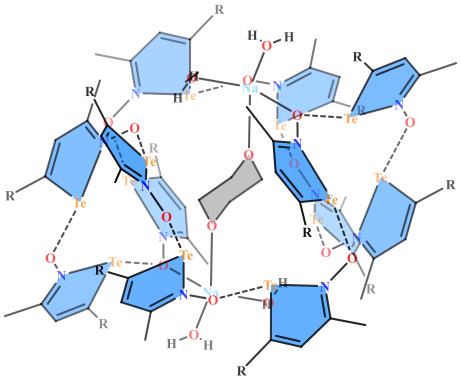

4

1,4-$C_4H_8O_2$⊂{$Na_2(H_2O)_4$(**1b**$_{12}$)}

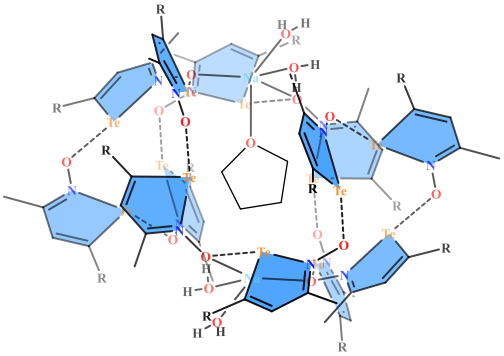

5

C_4H_8O⊂{$Na_2(H_2O)_4$(**1b**$_{12}$)}

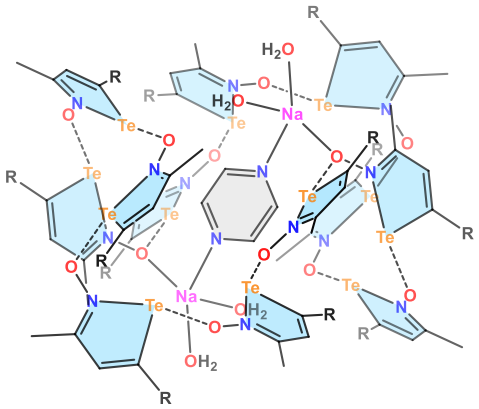

6

1,4-$C_4H_4N_2$⊂{$Na_2(H_2O)_4$(**1b**$_{12}$)

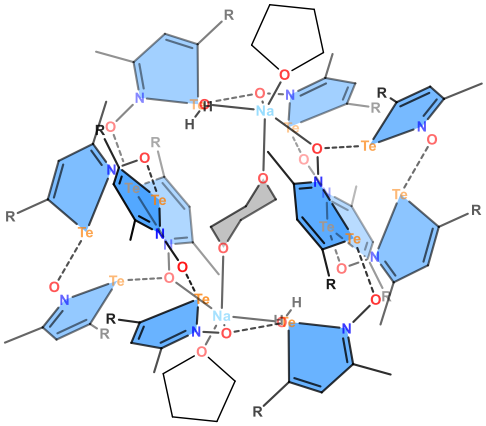

7
1,4-$C_4H_8O_2$⊂{$Na_2(H_2O)_2(THF)_2$(**1a**$_{12}$)}

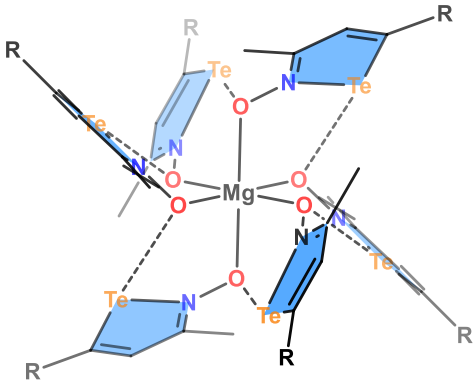

8a [Mg(**1a**$_6$)](BArF$_{24}$)$_2$
8b [Mg(**1b**$_6$)](BArF$_{24}$)$_2$

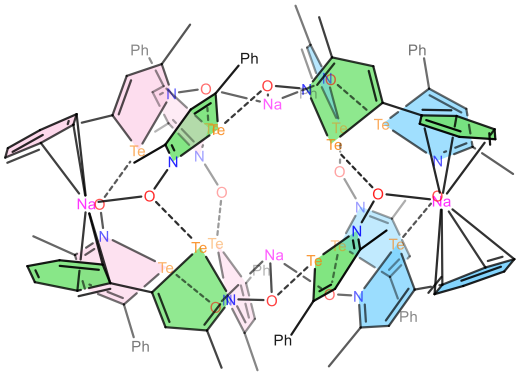

9
[Na_4(**1a**$_4$)$_3$](BArF$_{24}$)$_4$

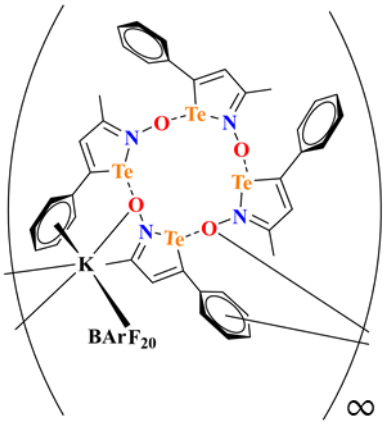

10
[K(**1a**$_4$)](BArF$_{20}$)

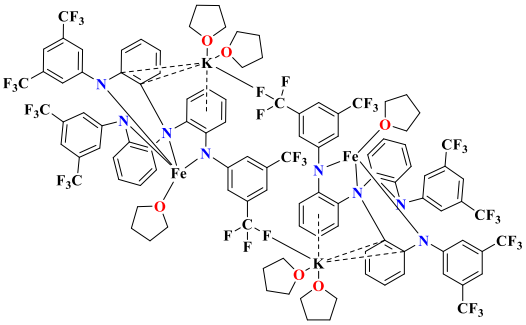

11

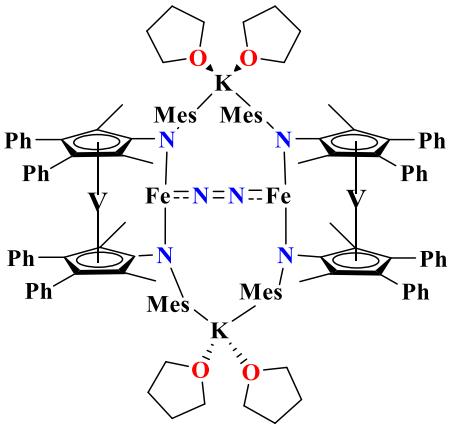

12

Chapter 1: Introduction

1.1 Macrocyclic ligands

Cyclic ligands bearing multiple electron donating atoms form very stable complexes with metal ions. This is due to favorable entropic contributions from the preorganization of donor atoms within the macrocycle as well as the displacement of multiple ligands by the macrocycle upon binding to a metal ion. Macrocycles and their complexes are a major branch of supramolecular chemistry.[1,2] An overwhelming majority of macrocyclic ligands contain hard donor atoms such as oxygen, and nitrogen (e.g. crown ethers, polyazacycloalkanes) because of their ability to form very stable complexes with metal ions.[1–4] Macrocycles containing heavier elements as donor atoms and their complexes have been studied to a lesser extent due to their weaker bonds to carbon and to metal ions.

Transition-metal complexes of selenium macrocycles have been reported and are known to be stable. In contrast, it has been difficult to construct tellurium macrocycles because of the large size of the atom and the high polarizability of the Te-C bond. Early examples of tellura-crown ethers include 1,5-ditelluracyclooctane and 1,5,9-tritelluracyclododecane.[5] However, these molecules could not form coordination complexes.[6,7] Another tellurium-centered molecule is 1,10-ditellura-4,7,13,16-tetraoxacyclooctadedecane which is capable of forming complexes with PtX_2, PdX_2 (X=Cl, Br), and $RhCl_3$.[8] The tellural-polyazamacrocycle coordinates Pd(II) by both Te and N atoms with a distorted square planar geometry.[9]

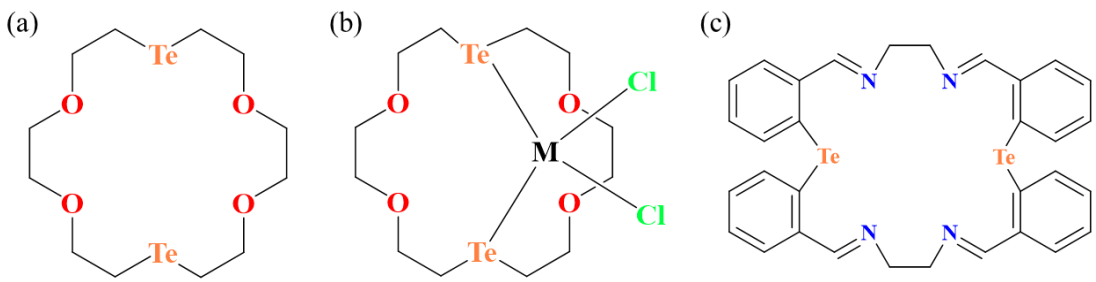

Figure 1.1 Structure of tellurium-containing macrocycles. (a) 1,10-ditellura-4,7,13,16-tetraoxacyclooctadedecane and (b) its complexes (M=Pd, Pt),[8] (c) is a tellural-polyazamacrocycle.[9]

1.2 Halogen bonding

Halogen atoms involved in covalent bonding interactions bear anisotropic electron density.[10] The belt region orthogonal to the covalent bond has higher electron density, and can act as electron donors. The region opposite to the covalent bond has a low electron density, this region is termed a sigma hole. This electrophilic region can attract electron-rich centres such as lone-pairs and π-electron clouds forming a secondary bonding interaction (SBI). This phenomenon usually results in a nearly linear geometric arrangement of the centre halogen atom and is termed halogen bonding. This is used to explain the unusual proximity observed between halogen atoms and adjacent electron donors. Intermolecular interactions such as hydrogen and halogen bonding can form a multitude of complex supramolecular motifs often in combination with reversible-covalent bonds and templating effects.[11,12] Although cyclic aggregates may be formed by multiple hydrogen or halogen bonds through templated reactions, there are no examples of macrocycles assembled through exclusively hydrogen or halogen bonding that are able to function as macrocyclic ligands towards metal ions.[13]

1.3 Chalcogen bonding

The remarkable success of halogen bonding in supramolecular chemistry has sparked great interest in the analogous secondary bonds formed by other heavy main group elements. Molecules that contain chalcogen (sulfur, selenium, and tellurium) atoms often exhibit this type of interaction. For instance, dichalcogena-alkynes form tubular structures in crystalline lattices,[14–16] and telluradiazoles are well known for their abilities to bind Lewis bases[17–21] and to form infinite ribbons in the solid state.[18,22] These concepts have recently been extended to the construction of benzotellurazole chains[23] and the development of tellurophenes capable of anion recognition[24] in solution. A unique development in this area, with no equivalent in halogen bonding, is the reversible auto association of iso-tellurazole-*N* oxide (**1**) through Te···O interactions into annular structures (**1a**$_4$, **1a**$_6$) that are persistent in solution and display chemical properties typical of actual macrocycles such as binding transition metal ions, forming fullerene adducts, and hosting small molecules.[25] A general summary of published work is shown in Scheme 1.1. Although Te-C bonds are known to be reactive and the preparation of **1** requires several steps that must be carried out under an inert atmosphere, the isolated compounds and their aggregates are stable in ambient conditions and are tolerant of water. Mineral acids such as HCl and HBr protonate the oxygen atom while the halide binds the chalcogen. The process is reversible and can be used to switch on and off the self-assembly.[26]

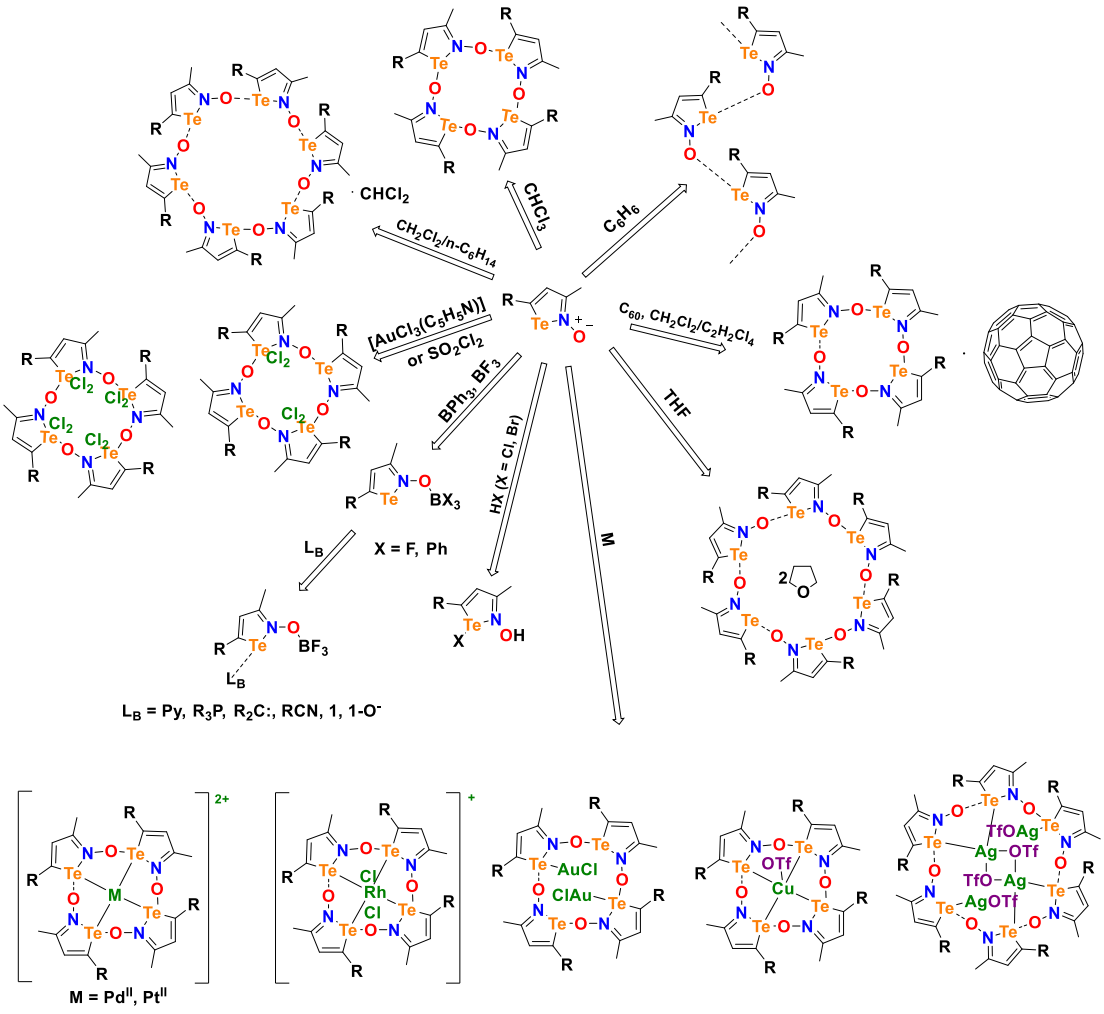

Scheme 1.1: Overview of the chemistry of iso-tellurazole *N*-oxides.

In the most general case, the auto-association of these molecules is a Lewis acid-base process, one in which oxygen is the electron donor and tellurium is the acceptor.[27] The self-assembly process of **1** can also be disrupted without halogen binding to the tellurium centre by reaction with BX_3 (X= F, Ph). This makes the most acidic site on the tellurium atom (the σ-hole along the extension of Te-N bond) available for other electron-donor atoms.

The Te atoms in macrocyclic tetramer can act as hosts for Pd(II), Pt(II) and Rh(III)

ion.[25,28] The crystal structure shows the coordination of the Pd(II) ion to the four Te atoms in a square planar geometry. The Te···O ChB is shortened from 2.299(2) Å to 2.172(8) Å and the Te-N bond is lengthened from 2.154(2) Å to 2.211 (9) Å, suggesting that the Pd(II) ion draws electron density from the tellurium atoms, making them more electrophilic towards the oxygen atoms. This complex was the first example of a metal ion coordinating to a macrocycle with only Te donor atoms. The Pt(II) analogue also displayed a similar square planar geometry and similar bond distances. The complex of **1** with Rh(III) was also synthesized, it has an octahedral geometry around the Rh(III) ion.

Recent investigations of the coordination chemistry of **1** with d^{10} metal ions revealed unique structures.[29] Both Cu(I) and Au(I) formed complexes with the tetramer, however, the crystal structure of Cu(I) showed an κ^4Te,κ^1O distorted square pyramidal coordination complex with the triflate anion in the apical position. The crystal structure of Au(I) contains a distorted chair tetramer. Two Te from coordinate an Au(I) ion each, while the other Te atoms engages in short contacts with the Au atom, a chloride anion completes a linear coordination sphere for each metal ion. No aurophilic interaction between Au atoms is observed in the crystal. The Ag(I) product is the first complex of the macrocyclic hexamer, it contains two silver atoms inside the ring bridged by two triflate anions, with a κ^2Te κ^2O tetrahedral coordination geometry and two more silver ions bound out of the ring, with a κ^1Te κ^1O κ^1C coordination sphere by bonding to the triflate anion and the aromatic carbon.

Despite the structural variations observed between the coordination complexes of **1** and the different transition metal ions, coordination had only been observed to Te, however, the oxygen atoms is a good donor especially towards hard metal ions. As a result, O-coordination could compete with the Te···O chalcogen bond. This project is intended to establish which metal ions coordinate to oxygen and the effect they have on the Te···O chalcogen bonds. Experimental work with hard metal ions of alkali metals and alkaline earths revealed novel macrocyclic complexes. The new compounds were characterized by X-ray crystallography and NMR spectroscopy. The counterions of choice belong to the $BArF^-$ family of weakly coordinating anions.

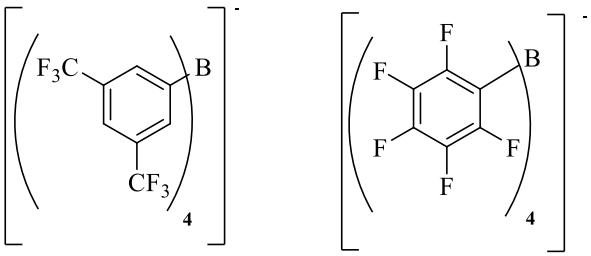

2a **2b**

Figure 1.2: Lewis structure of two variants of the weakly coordinating anions $BArF^-$.

Chapter 2: Experimental

2.1 Materials and Methods

The manipulation of air-sensitive materials was carried out in a glovebox or standard Schlenk techniques under atmospheres of anhydrous nitrogen or argon. All glassware was dried at 140ºC in an oven. Organic solvents were purified by distillation over the Na^0/benzophenone or CaH_2. $K(BArF_{20})$ were heated to 120° under dynamic vacuum for 12 hours prior to use.

The following compounds were received from suppliers: potassium tetrakis(pentafluorophenyl)borate (Boulder Scientific), d_2-dichloromethane (Cambridge Isotope Laboratories) and $CDCl_3$ (Cambridge Isotope Laboratories).

The following compounds were prepared following literature methods: 3-methyl-5-phenyl-1,2-tellurazole 2-oxide, 3-Methyl-5-[(3,5-di-tert-butyl)phenyl]-1,2-tellurazole 2-oxide,[28] $MBArF_{24}$ ($M=Li^+$, Na^+, K^+, Rb^+, Cs^+),[30–32] $M(BArF_{24})_2$ ($M=Mg^{2+}$, Ca^{2+}).[33]

2.2 Instrumental Methods

2.2.1 Nuclear Magnetic Resonance Spectroscopy

NMR spectra were collected using Bruker AVANCE 500 MHz or 600 MHz spectrometer at 298 K; The ^1H and ^{13}C spectra were processed using Bruker TopSpin 4.0 software and were referenced to deuterated solvent.

Sample preparation

All samples were prepared by dissolving approximately 5mg of the compound in 0.5mL of deuterated solvent.

2.2.2 Single Crystal X-ray Diffraction

Sample Preparation

X-ray data were collected on a Bruker SMART APEX II diffractometer equipped with an APEX II 4K CCD area detector, using either a graphite monochromator or a Bruker Triumph curved crystal monochromator Mo-Kα radiation (λ=0.71073) at 100(2) K. Samples were handled at room temperature coated in Paratone-N oil, suitable crystals were mounted on a nylon loop.

Data Treatment

Once the data collection was completed, the structures were solved using the SHELXTL[34] suite of programs and most structures were refined by full-matrix least square of all F^2 values with the WinGX package. The data was empirically corrected for absorption and other effects using SADABS. The non-H atoms were refined anisotropically, while H atoms were constrained to idealized positions using appropriate riding models. Molecular graphics were produced using the Cambridge Crystallographic Data Centre's Mercury package versions 2020.1.[35]

2.2.3 IR Spectroscopy

Infrared spectra were recorded using Smart iTX attenuated total reflectance (ATR) sample analyzer equipped on Thermo Scientific Nicolet 6700 FT-IR spectrometer.

2.2.4 Elemental Analysis

Combustion elemental analyses were carried out by the London Metropolitan University Elemental Analysis Service (London, United Kingdom).

2.2.5 Melting Point

Melting points were measured on a Thomas-Hoover melting point apparatus and are reported uncorrected.

2.3 Computational Details

Density Functional Theory calculations were performed using the Software for Chemistry & Materials Amsterdam Density Functional package versions 2019.3. The adiabatic local density approximation (ALDA) was used for the exchange correlation kernel, and the differentiated static LDA expression was used with the Vosko-Wilk-Nusair parameterization. The calculations of model geometries were gradient corrected with the exchange and correlation functionals of the gradient correction proposed by Perdew and Wang.[36] Preliminary geometry optimizations were performed using a double-ζ basis set without frozen cores corresponding to the configuration of the preceding noble gas and no polarization functions; the resulting structures were refined by using a triple-all-electron basis set with one polarization function and applying the zeroth order relativistic approximation (ZORA) with the specially adapted basis sets. The effect of dispersion forces was examined with the use of the Perdew-Burke-Ernzerhoff (PBE)[37] functional supplemented by Grimme's D3 correction.[38]

2.4 Syntheses

C_6H_{12}⊂{1a$_{12}$} (3): 1a (10 mg) was dissolved in 1 mL of CH_2Cl_2 and subjected to liquid-liquid diffusion with cyclohexane. Yield: 20%; mp: 195-208°C (dec.); ^{1}H-NMR (600MHz, CD_2Cl_2) (δ ppm): 7.25-7.43 (m, 60H), 7.10 (s, 12H), 1.71(s, 36H), 1.44(s, 12H); ^{13}C NMR (500MHz, CD_2Cl_2) (δ ppm): 158.0, 154.1, 140.3, 129.7, 128.1, 127.9,

127,6, 27.43, 16.1; ^{125}Te NMR resonance could not be observed due to low solubility of the compound; IR (ATR): 3049.16, 2930.43, 2915.22, 2987.30, 2198.31, 2032.57, 1567.92,1492.15, 1450.5, 1373.92, 1221.61, 1103.31, 1025.82925.53, 843.89, 757.69, 697.90 cm^{-1}. E.A. Anal. Calcd for $C_{126}H_{120}N_{12}O_{12}Te_{12}$: C,42.92; H,3.43; N,4.77. Found: C, 42.99: H,3.19; N,4.76.

General method for isolation of sodium containing dodecamers:

The procedure can be adapted for all sodium-dodecamer complexes. Na(BArF)(0.004mM) and **1a/b** (0.024mM, 6 mol equiv.) were mixed in 1mL CH_2Cl_2, and allowed to stir for 18 hours followed by the addition of 0.002mM of guest molecule. The mixture was then stirred for another 5 hours, followed by filtration, and subjected to liquid-liquid diffusion with n-hexanes at room temperature for two weeks.

1,4-$C_4H_8O_2$⊂{$Na_2(H_2O)_4$(1b_{12})} (**4**): Yield: 55%; mp: 188°C (dec.); ^{1}H (600MHz, CD_2Cl_2) (δ ppm): 7.7174(m, 16H), 7.5573(s, 8H), 7.4190(m, 12H), 7.1839(s, 12H), 7.1499(m, 24H), 3.6466 (s, 8H), 1.7729 (s, 36H), 1.51(s, 8H), 1.2913(s, 216H); ^{13}C NMR (500MHz, CD_2Cl_2) (δ ppm): 162.19, 159.46, 151.15, 138.37, 135.21, 129.28, 127.32, 125.92, 124.12, 123.64, 123.25, 122.31, 117.87, 67.48, 16.14. ^{125}Te NMR resonance could not be observed; IR (ATR): 3360, 2953, 2874, 1562, 1497, 1381, 1294, 1135, 873, 847, 709, 684. E.A. Anal. Calcd for $C_{284}H_{340}N_{12}O_{18}Te_{12}B_2Na_2F_{48}$: C,50.76; H,5.1; N,2.5. Found: C, 50.45: H,4.87; N,2.16.

C_4H_8O⊂{$Na_2(H_2O)_4$(1b_{12})} (5): Yield: 51%; mp: 187°C (dec.); ^{1}H (600MHz, CD_2Cl_2) (δ ppm): 7.7174(m, 16H), 7.5573(s, 8H), 7.4430(t, 12H), 7.1430(t, 12H), 7.1423(d, 24H), 3.6973 (m, 8H), 1.8201 (m, 4H), 1.7729 (s, 36H), 1.2913(s, 216H); ^{13}C

NMR (500MHz, CD_2Cl_2) (δ ppm): 162.03, 159.86, 151.17, 138.80, 135.19, 129.42, 127.26, 125.28, 123.66, 123.24, 122.83, 122.31, 117.93, 67.48, 31.58, 16.14. ^{125}Te NMR resonance could not be observed; IR (ATR): 3315, 2987, 2883, 1596, 1483, 1367, 1323, 1104, 986, 903, 886, 747, 724; E.A. Anal. Calcd for $C_{284}H_{340}N_{12}O_{17}Te_{12}B_2Na_2F_{48}$: C,50.88; H,5.11; N,2.51. Found: C, 51.19: H,4.74; N,2.29.

1,4-$C_4H_4N_2$⊂{$Na_2(H_2O)_4$(1b$_{12}$)} (6): Yield: 20%; mp: 187°C (dec.); ^{1}H (600MHz, CD_2Cl_2) (δ ppm): δ 8.5324(s, 4H), 7.7174(m, 16H), 7.5573(s, 8H), 7.7430(t, 12H), 7.7430(t, 12H), 7.1423(d, 24H), 1.8201 (m, 4H), 1.7729 (s,36H), 1.2913(s,216H); ^{13}C NMR (500MHz, CD_2Cl_2) (δ ppm): 162.43, 159.79, 151.65, 138.24, 135.98, 129.12, 127.45, 125.32, 123.34, 123.14, 122.12, 122.51, 117.83, 67.83, 31.82, 16.19. ^{125}Te NMR resonance could not be observed; IR (ATR): 3066, 2122, 1582, 1434, 1113, 938, 740, 690, 512, 487. Satisfactory elemental analysis result has not yet been obtained.

1,4-$C_4H_8O_2$⊂{$Na_2(H_2O)_2(THF)_2$(1a$_{12}$)} (7): A few crystals suitable for x-ray diffraction were isolated following the general procedure, but sizeable quantities of analytically pure product could not be obtained. Multiple attempts to isolate the pure product by altering crystallization condition were not successful. Further optimizations on the isolation of this product are needed.

[Mg(1a$_6$)](BArF$_{24}$)$_2$(8a): [Mg(MeCN)$_6$](BArF$_{24}$)$_2$ (1 equiv.) and **1a** (6 equiv.) were mixed in 1mL CH_2Cl_2 and allowed to stir for 18 hours, followed by high vacuum to dryness and re-dissolved in CH_2Cl_2 to stir for another 5 hours. The solution was filtered through celite plug and subjected to liquid-liquid diffusion with hexane to afford orange crystals. Yield: 86%; mp: 196°C (dec.); ^{1}H (600MHz, CD_2Cl_2) (δ ppm):

7.7483(m, 32H), 7.5841(s, 6H), 7.5616(m, 16H), 7.4026(m, 30H), 2.2303(s, 18H); ^{13}C NMR (500MHz, CD_2Cl_2) (δ ppm): 162.13, 160.72, 154.34, 135.30, 134.88, 129.16, 128.24, 124.78, 123.87, 123.34, 122.34, 122.61, 118.16, 16.96; ^{125}Te NMR resonance could not be observed. IR (ATR):3049, 2917, 1568, 1492, 1373, 1103, 1026, 925, 783, 697, 623, 583. E.A. Anal. Calcd for $C_{124}H_{78}N_6O_6Te_6B_2Mg_1F_{48}$: C, 42.9; H, 2.26; N, 2.42. Found: C, 43.22: H, 2.31; N, 2.21.

[Mg(1b)$_6$](BArF$_{24}$)$_2$(8b): As for the **1a** analogue, use **1b** (6 equiv.). Yield: 12%; ^{1}H (600MHz, CD_2Cl_2) (δ ppm); 7.71(m, 32H), 6.771-7.42(m, 24H), 2.16(s, 18H), 1.21(s, 108H). Satisfactory elemental analysis result has not yet been obtained.

[Na$_4$(1a)$_{12}$](BArF$_{24}$)$_4$(9): Yield: 5%; Na(BArF)(0.0012mM) and **1a** (0.036mM, 3 mol equiv.) were mixed in 1mL CH_2Cl_2, and allowed to stir for 24 hours followed by filtration using celite plug then subjected to liquid-liquid diffusion with n-hexanes at room temperature. Thin plates were observed after two weeks. ^{1}H (600MHz, CD_2Cl_2): δ 7.7188(s, 64H), 7.5578(m, 32H), 7.4155-7.1435(m, 72H), 1.7398 (s, 36H). ^{13}C NMR and ^{125}Te NMR resonances could not be observed due to the low solubility of the compound. Sizable quantities of analytically pure product for EA analysis could not be obtained, crystals are thin-layered and surrounded by starting material crystals. Further optimizations on the isolation of this product are needed.

[K(1a$_4$)](BArF$_{20}$)(10): $KBArF_{20}$ and **1a** were mixed in 1mL fluorobenzene for 10 mins, followed by filtration and subjected to liquid-liquid diffusion with n-hexane at room temperature. Prolonged mixing induced precipitation of the pure material. The material is not soluble enough to acquire meaningful ^{1}H, ^{13}C and ^{125}Te NMR data. E.A.

Anal. Calcd for $C_{124}H_{78}N_6O_6Te_6B_2Mg_1F_{48}$: C, 41.21; H, 1.95; N, 3.00. Found: C, 41.51: H, 1.89; N, 3.03.

2.5 Summary of Crystallographic Data

Table 2.1 Crystallographic and refinement data for all compound

Crystal Composition	$C_6H_{12}\subset\{1a_{12}\}$ (**3**)	$[1,4\text{-}C_4H_8O_2\subset\{Na_2(H_2O)_4(\mathbf{1b}_{12})\}]$ (**4**)	$[C_4H_8O\subset\{Na_2(H_2O)_4(1b_{12})\}$ (**5**)	$[1,4\text{-}C_4H_4N_2\subset\{Na_2(H_2O)_4(1b_{12})\}]$ (**6**)	$[1,4\text{-}C_4H_8O_2\subset\{Na_2(H_2O)_2(THF)_2(1a_{12})\}]$ (**7**)
Empirical formula	$C_{120}H_{108}N_{12}O_{12}Te_{12}$	$C_{286}H_{344}N_{12}Na_2O_{18}Te_{12}B_2F_{48}Cl_4$	$C_{286}H_{344}N_{12}Na_2O_{17}Te_{12}B_2F_{48}Cl_4$	$C_{296}H_{362}N_{14}Na_2O_{16}Te_{12}B_2F_{48}$	$C_{296}H_{362}N_{14}Na_2O_{16}Te_{12}B_2F_{48}$
Crystal system	Trigonal	Triclinic	Triclinic	Triclinic	Triclinic
Space Group	R-3	P-1	P-1	P-1	P-1
a (Å)	19.057(3)	18.1596(10)	18.338(2)	18.374(1)	17.398(7)
b(Å)	19.057(3)	20.6229(12)	20.749(3)	20.8491(11)	19.891(8)
c(Å)	31.746(5)	24.4995(14)	24.307(3)	24.2216(12)	20.581(9)
α (°)	90	104.263(2)	104.173(2)	104.240(3)	108.918(8)
β (°)	90	110.263(2)	110.015(2)	109.721(3)	111.196(7)
γ (°)	120	102.519(2)	103.288(2)	103.727(3)	92.776(8)
V (Å^3)	9984(3)	7868.08	7910.8(18)	7927.3(7)	6170(4)
Z, p(calc.) [g. cm^{-3}]	3,1.801	1, 1.241	1, 1.451	1, 1.442	1, 1.458
u (mm^{-1})	2.648	1.181	1.216	1.174	1.485
Limiting indices	-23<h<23	-22<h<22	-22<h<22	$-26 \le h \le 26$	$-21 \le h \le 21$
	-23<k<23	-25<k<25	-25<k<25	$-29 \le k \le 29$	$-24 \le k \le 24$
	-39<l<39	-30<l<30	-30<l<30	$-34 \le l \le 34$	$-25 \le l \le 25$
R_{int}	0.1892	0.1048	0.0745	0.3367	0.2914
No. of parameters	255	1869	1883	1922	1367
R_1*/wR_2*(I>2σ(I))	0.0476/0.1212	0.0592/0.1432	0.0525/0.1119	0.0824/0.1504	0.1190/ 0.2902
R_1*/wR_2* for all data	0.0856/0.1490	0.1253/0.1907	0.0961/0.1361	0.2807/0.2198	0.2681/ 0.3675
Goodness of fit on F^2	0.956	0.994	1.07	0.936	1.053

$R_1=\Sigma||F_o|-|F_c||/\Sigma|F_o|$, $wR2=\{\Sigma[w(F_o^2-F_c^2)^2]/\Sigma w(F_o^2)^2\}$

Table 2.1 Crystallographic and refinement data for all compound (continues)

Crystal Composition	[Mg(**1a**$_6$)](BArF)$_2$(**8a**)	[Mg(**1b**$_6$)](BArF)$_2$(**8b**)	[Na$_4$(**1a**$_4$)$_3$](BArF$_{24}$)$_4$(**9**)	[K(**1a**$_4$)](BArF$_{20}$)(**10**)
Empirical formula	$C_{124}H_{78}B_2F_{48}MgN_6O_6Te_6$	$C_{172}H_{174}B_2F_{48}MgN_6O_6Te_6$	$C_{248}H_{156}N_{12}O_{12}Te_{12}B_4Na_4F_{96}$	$C_{64}H_{36}N_4O_4Te_4KBF_{20}$
Crystal system	Triclinic	Triclinic	triclinic	Monoclinic
Space Group	P-1	P-1	P-1	$P2_1/c$
a (Å)	13.354(8)	17.8416(10)	19.657(2)	14.057(2)
b(Å)	15.774(10)	18.0549(10)	21.893(2)	16.005(3)
c(Å)	17.156(11)	18.3889(10)	34.314(4)	31.746(5)
α (°)	115.205(6)	84.493(3)	96.250(2)	90
β (°)	97.252(6)	64.053(3)	94.584(2)	92.894(2)
γ (°)	97.056(6)	72.307(3)	115.549(2)	90
V (Å^3)	3180(3)	5069.8(5)	13111(2)	7133.4(19)
Z, p(calc.) [g. cm^{-3}]	1, 1.813	1, 1.358	2/1.572	1, 13.105
u (mm^{-1})	1.490	0.947	1.413	12.968
Limiting indices	-17<h<17	-22<h<22	-17 ≤ h ≤ 17	-20 ≤ h ≤ 19
	-20<k<20	-22 ≤ h ≤ 22	-19 ≤ k ≤ 19	-22 ≤ k ≤ 22
	-22<l<22	- -22 ≤ h ≤ 22	-31 ≤ l ≤ 31	-45 ≤ l ≤ 45
R_{int}	0.1908	0.1656	0.1176	0.1422
No. of parameters	874	1201	1525	904
R_1*/wR_2*(I>2σ(I))	0.0647/ 0.0936	0.0570/ 0.1107	0.1101/ 0.2874	0.1678/ 0.3341
R_1*/wR_2* for all data	0.1708/ 0.1228	0.1193/ 0.1285	0.1919/ 0.3335	0.2195/ 0.3577
Goodness of fit on F^2	1.036	1.006	0.987	1.159

$R_1=\Sigma||F_o|-|F_c||/\Sigma|F_o|$, $wR2=\{\Sigma[w(F_o^2-F_c^2)^2]/\Sigma w(F_o^2)^2\}$

Chapter 3: Study of Na-containing dodecamers of iso-tellurazole *N*-oxide

3.1 Introduction

The key player in the self-assembly of iso-tellurazole *N*-oxide in solution is the chalcogen bonding interaction between the oxygen and the tellurium atoms of distinct molecules. Due to the reversible nature of the self-assembly of these small molecules in solution, initial studies were conducted by Ho *et al.* to understand their dynamic character.[25] Notably, the NMR data suggested that two-species are in equilibrium at low temperature, with the equilibrium affected by both temperature and concentration, and crystal structures of **1a$_\infty$, 1a$_4$, 1a$_6$** were all isolated by changing the crystallization conditions. Through scrambling experiments with **1** bearing different R-functional groups, the observed NMR pattern and its dependency on the composition of a mixture pointed to the annular tetramers, a further concentration study identified the emergence of hexamers at low temperature. A computational thermodynamic study showed that the hexamer is enthalpically favorable, while the tetramer is entropically more favorable, in agreement with the observations made by NMR. However, the electrospray mass spectrum displayed isotopic patterns of [**1a**$_n$-H]$^+$, where n=1-7, implying hexamer might not be the limit of aggregation in solution and larger oligomers are possible. In this chapter, we will introduce a dodecameric structure initially discovered during attempts to crystalize a Cs^+ complex.

3.2 Result and discussion

3.2.1 Synthesis

A novel macrocyclic organization was uncovered by stirring $NaBArF_{24}$ with **1a/1b** in CH_2Cl_2 with stoichiometry guest molecules (dioxane, THF and pyrazine) for 16 hours in inert atmosphere followed by liquid-liquid diffusion using CH_2Cl_2/hexane. This resulted in yellow crystals that were isolated and identified by single-crystal X-ray diffraction. The compound readily dissolves in CH_2Cl_2. Synthesis using $LiBArF_{24}$, $KBArF_{24}$, $RbBArF_{24}$ and $CsBArF_{24}$ resulted in the crystallization of the salt and the ligand as either $\mathbf{1}_{\infty}$, $\mathbf{1}_4$ or $\mathbf{1}_6$ depending on the conditions. However, crystallization with $CsBArF_{24}$ and **1a** afforded crystalline of $C_6H_{12}\subset\{\mathbf{1a}_{12})\}$ after CH_2Cl_2 /hexane diffusion. The same crystal was later isolated using only **1a** with CH_2Cl_2 /cyclohexane diffusion. The crystals of $C_6H_{12}\subset\{\mathbf{1a}_{12}\}$, $[1,4\text{-}C_4H_8O_2\subset\{Na_2(H_2O)_4(\mathbf{1b}_{12})\}]$, $C_4H_8O\subset\{Na_2(H_2O)_4(\mathbf{1b}_{12})\}$, $1,4\text{-}C_4H_4N_2\subset\{Na_2(H_2O)_4(\mathbf{1b}_{12})\}$ and $1,4\text{-}C_4H_8O_2\subset\{Na_2(H_2O)_2(THF)_2(\mathbf{1a}_{12})\}$ all form 12 N-Te···O linkages. Due to the structural similarity, the discussion will begin with the simpler structure, $C_6H_{12}\subset\{\mathbf{1a}_{12}\}$.

3.2.2 Crystal structure

Crystallographic and refinement data for the dodecamers of iso-tellurazole *N*-oxide are presented in Table 2.1, and selected distances and angle are presented in Table 3.1

3.2.3 $C_6H_{12}\subset\{1a_{12}\}$

Initially isolated as a side-product, **1a** selectively crystallized with cyclohexane from reagent grade hexane solvent. Using CH_2Cl_2 /cyclohexane led to direct isolation of this product. The ligand forms a novel cyclic dodecamer (Figure 3.1), and the crystal

features a circular $(N\text{-}Te\cdots O)_{12}$ linkage, which folds onto itself, rendering a cavity in the middle of the macrocycle that in this case is occupied by a molecule of cyclohexane. The encapsulated cyclohexane displays chair conformation. The N-Te···O linkage maps the inner shell of the cavity while the carbon skeleton of the ligand flanks on the outside (Figure 3.2). The crystals have poor solubility in most organic solvent.

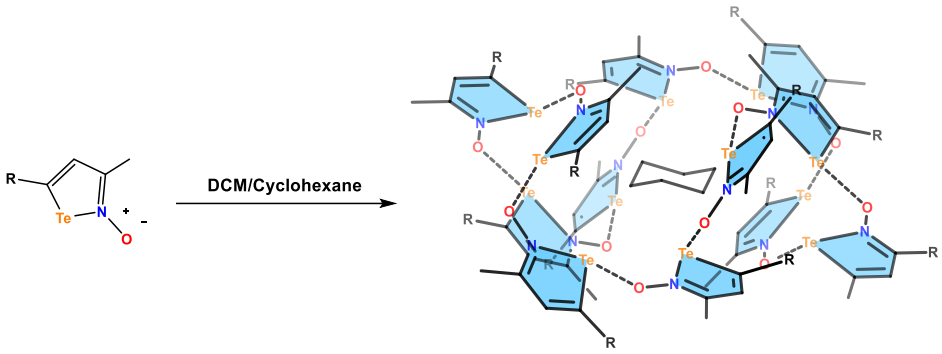

Scheme 3.1: Synthesis of $C_6H_{12}\subset\{\mathbf{1a}_{12}\}$.

While the unit cell comprises three dodecamers, the asymmetric unit consists only of two molecules of **1a** and one CH_2 fragment. The whole structure of the aggregate is therefore generated by the symmetry operations of the S_6 point group. The $d(Te\cdots O)_{dodecamer}$ distances are 2.204(4) and 2.259(7)Å, in contrast to $d(Te\cdots O)_{polymer}$ = 2.176(4)-2.208(4) Å; $d(Te\cdots O)_{tetramer}$ = 2.203(1), 2.242(1) Å, $d(Te\cdots O)_{hexamer}$ = 2.171(3)-2.178(2) Å. The $d(Te\cdots O)_{dodecamer}$ on average is comparable to the tetramer but is slightly longer when compared to the polymer or hexamer. The $d(Te\text{-}N)_{dodecamer}$ and $d(Te\text{-}C)_{dodecamer}$ follows similar trend, however, the Te···Te distances between neighbouring heterocycles range from 3.631(1)-3.634(1)Å, in contrast to $d(Te\text{-}Te)_{polymer}$=3.7403(6)-3.7887(8) Å; $d(Te\text{-}Te)_{tetramer}$= 3.8426(4), 3.8633(2) Å, d(Te-

Te)$_{hexamer}$ =3.6856(7)-3.7229(7)Å. This shortening suggests the higher aggregation brings relief of ring strain, with respect to the smaller macrocycles. The interplanar angle constituted by adjacent ligand ranges from 70.7(5)°-80.3(6)° similar to the other observed **1a** aggregates.

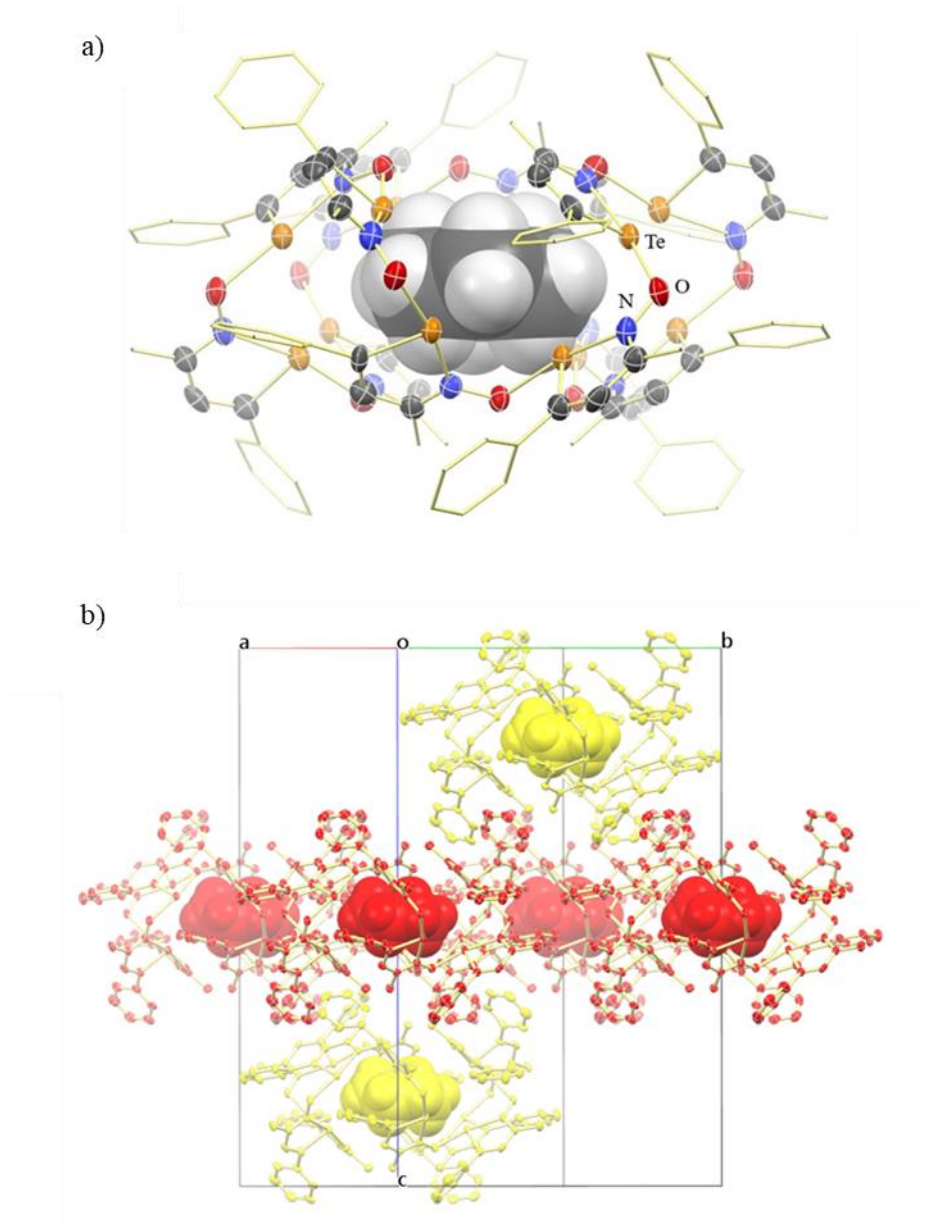

Figure 3.1: Crystal structure of $C_6H_{12}\subset\{\mathbf{1a}_{12}\}$. a) Molecular structure of the host-guest complex. b) unit cell contents. Each two yellow colored molecule represents a dodecamer, and each of four red colored dodecamers contribute to the third dodecamer

in the unit cell. Hydrogen atoms of **1a** are omitted for clarity.

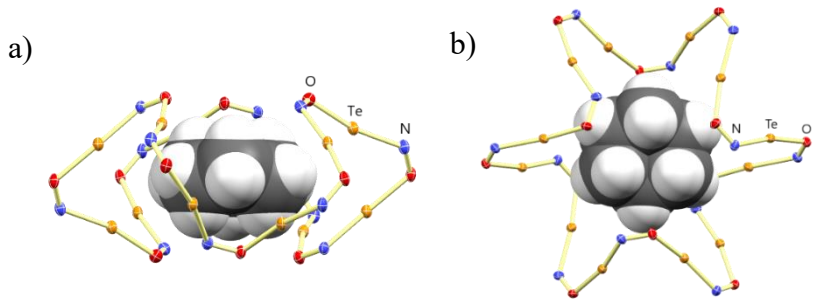

Figure 3.2: Detail of the crystal structure of $C_6H_{12}\subset\{\mathbf{1a}_{12}\}$. Carbon and hydrogen atoms of the ligand are omitted for clarity. a) viewing along c axis. b) view along the a axis.

3.2.4 [1,4-$C_4H_8O_2\subset\{Na_2(H_2O)_4(\mathbf{1b}_{12})\}$]

Crystals suitable for X-ray analysis were isolated using $Na(BArF_{24})$, which established the composition [1,4-$C_4H_8O_2\subset\{Na_2(H_2O)_4(\mathbf{1b}_{12})\}$]. The two sodium ions are on opposite poles of the dodecamer and are κ^5O coordinated with a distorted square pyramidal geometry, each is coordinated by two oxygen from the **1b** dodecamer, two water molecules, and one oxygen from the dioxane molecule (Figure 3.3). Coordination to the oxygen atom of **1b** does not cause dissociation of the Te···O ChB. The unit cell in this case contains only one dodecamer and the two anions on opposite corners. Although bearing similar N-Te···O ChBs to those in $C_6H_{12}\subset\{\mathbf{1a}_{12}\}$ (Figure 3.4), the symmetry of the molecule is reduced by the coordination of O1 and O2 to Na. Notably, the Te···O distance in [1,4-$C_4H_8O_2\subset\{Na_2(H_2O)_4(\mathbf{1b_{12}})\}$] spans a wide range from 2.188(4) Å to 2.302(3) Å, where the longest ChB distance corresponds to the oxygen

with bifurcated coordination to Na^+, however, the average d(Te···O) is still comparable to those in $C_6H_{12}\subset\{\mathbf{1a}_{12}\}$. Coordination to oxygen lengthens the ChB, but it does not break this interaction. The solid remains crystalline after two hours under dynamic vacuum (105 mTorr). The water molecules in the crystal structure are likely from trace amounts present in the starting materials.

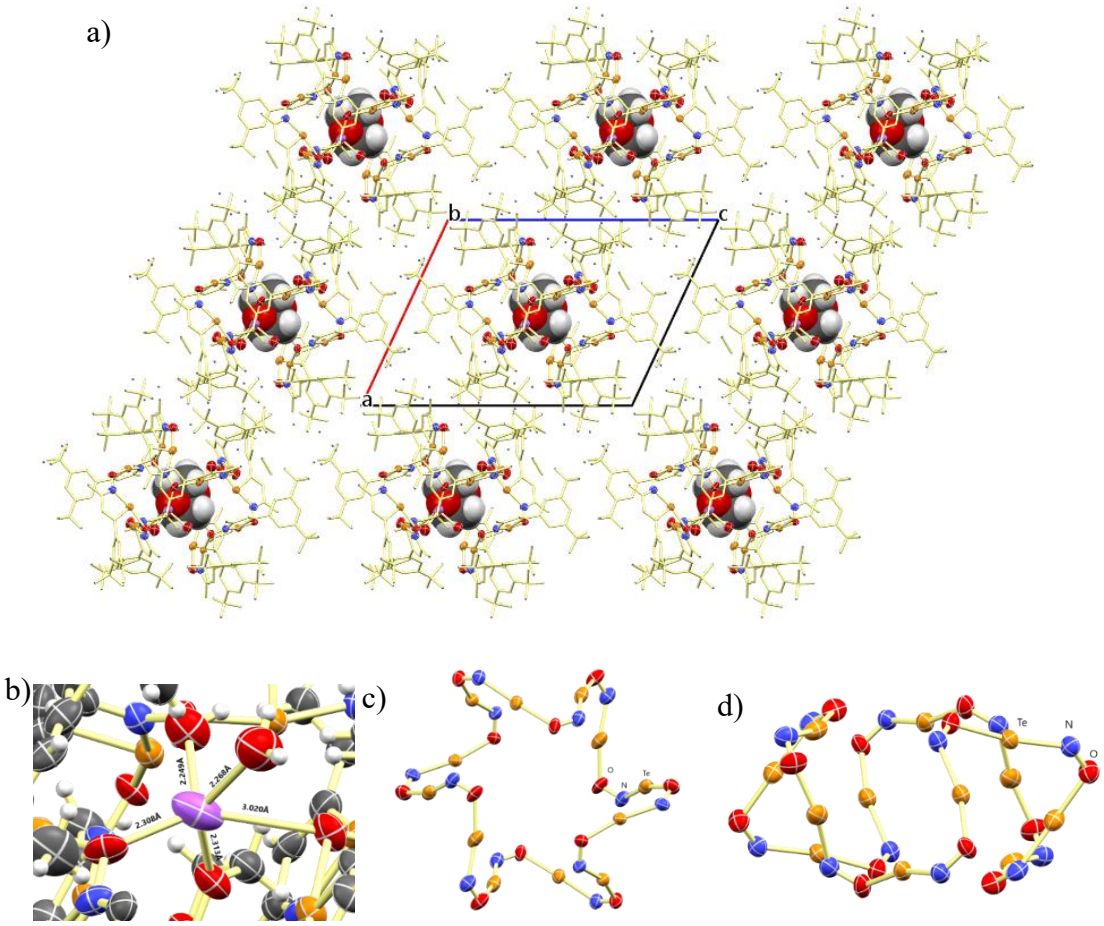

Figure 3.3: Crystal structure of [1,4-$C_4H_8O_2\subset\{Na_2(H_2O)_4(\mathbf{1b}_{12})\}$]. Hydrogen atoms of the complex and anions are omitted for clarity. a) Packing of [1,4-$C_4H_8O_2\subset\{Na_2(H_2O)_4(\mathbf{1b}_{12})\}$]. b) The sodium cation (purple) coordinated by two oxygen from two water molecules, two oxygen from ligand and one oxygen from the guest molecule. c)&d) two views of the macrocycle backbone, hydrogen and carbon atoms are omitted for clarity. Ellipsoids are shown at 75% probability.

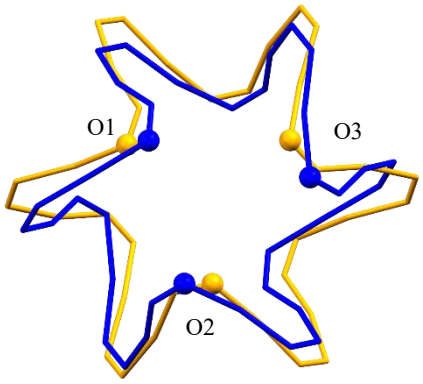

Figure 3.4: Overlay of the $(N\text{-}Te\cdots O)_{12}$ backbones of $C_6H_{12}\subset\{\mathbf{1a_{12}}\}$(yellow) and [1,4-$C_4H_8O_2\subset\{Na_2(H_2O)_4(\mathbf{1b_{12}})\}$] (blue) in sticks, the axial oxygen atoms are shown as spheres to illustrate their displacement uponcoordination to Na^I.

3.2.5 [$C_4H_8O\subset\{Na_2(H_2O)_4(\mathbf{1b_{12}})\}$ and [1,4-$C_4H_4N_2\subset\{Na_2(H_2O)_4(\mathbf{1b_{12}})\}$]

The THF-dodecamer complex also crystalized in P-1 space group. Despite there being one less oxygen atom in the guest occupying the cavity, the dodecamer is still bound to two sodium ions. These are coordinated κ^2O to $\mathbf{1b}_{12}$ and two water molecules, but only one is also bonded to the oxygen of the THF molecule. As a result, the crystal shows 50% disorder on the orientation of the encapsulated THF molecule and the position of the two Na ions. The pentacoordinated sodium ion is closer to the centre of the structure, leaving the two sodium ions crystallographic independent (Figure 3.5a). Bond distances and bond angles are comparable to those in [1,4-$C_4H_8O_2\subset\{Na_2(H_2O)_4(\mathbf{1b_{12}})\}$], in spite of THF being a smaller molecule than dioxane. Crystallization with pyrazine led to the isolation of [1,4-$C_4H_4N_2\subset\{Na_2(H_2O)_4(\mathbf{1b_{12}})\}$]

(Figure 3.5b), which has a backbone similar to those of the dioxane and THF complexes. Satisfactory elemental analysis results were not obtained for the pyrazine complex despite multiple attempts on crystal growth. All three crystals of the dodecamer with Na^+ are nearly isomorphic.

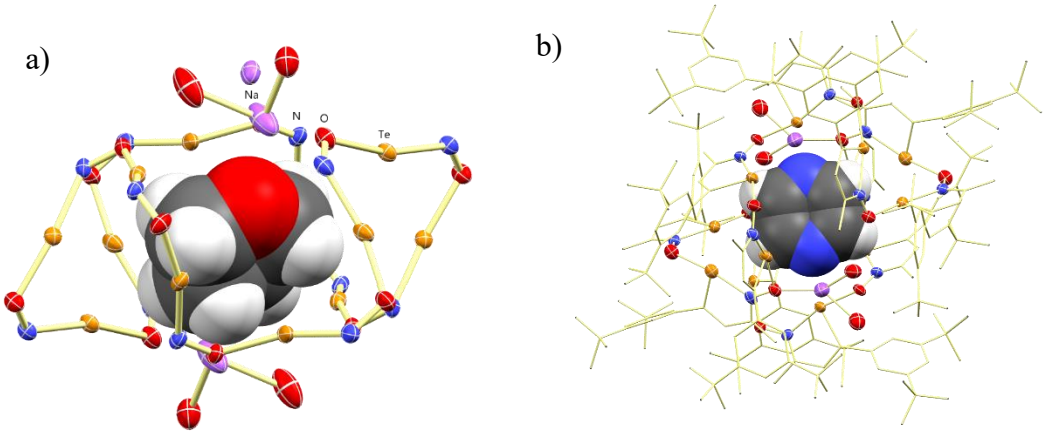

Figure 3.5: Crystal structure of [1,4-C_4H_8O⊂{$Na_2(H_2O)_4$(**1b**$_{12}$)}] (a) and [1,4-$C_4H_4N_2$⊂{$Na_2(H_2O)_4$(**1b**$_{12}$)}] (b). a) the two possible positions of the sodium ion (purple) depending on the orientation of the THF molecule is illustrated. Carbon and hydrogen atoms of **1b** are omitted for clarity. b) ORTEP of [1,4-$C_4H_4N_2$⊂{$Na_2(H_2O)_4$(**1b**$_{12}$)}], hydrogen atoms are omitted for clarity.

3.2.6 [1,4-$C_4H_8O_2$⊂{$Na_2(H_2O)_2(THF)_2$(**1a**$_{12}$)}]

Despite the successful isolation of C_6H_{12}⊂{**1a**$_{12}$}, in contrast to **1b**, the **1a**$_{12}$-Na complex had a much lower yield. The crystal structure obtained with **1a** was [1,4-$C_4H_8O_2$⊂{$Na_2(H_2O)_2(THF)_2$(**1a**$_{12}$)}]. The space group is P-1, as the other isolated Na-dodecamers complexes. The unit cell dimensions are slightly shorter in all a, b and c dimensions due to the lack of t-butyl groups. The N-Te···O ChBs remain consistent,

however, the pentacoordinated Na^+ ion is bound to one THF and one water molecule instead of two water molecules (Figure 3.6), compared to the structure of [1,4-$C_4H_8O_2$⊂{$Na_2(H_2O)_4$(**1b**$_{12}$)}]. The water molecule fulfills the coordination sphere of the Na^+ ion but it is not constrained to a fixed position in the coordination sphere.

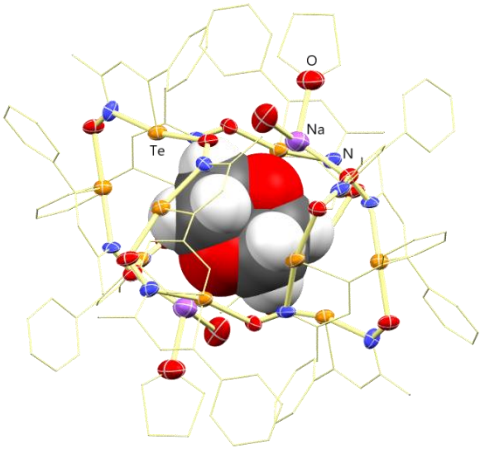

Figure 3.6: Crystal structure of [1,4-$C_4H_8O_2$⊂{$Na_2(H_2O)_2(THF)_2$(**1a**$_{12}$)}].

Table 3.1 Selected structural data

Crystal	3	4	5	6	7
Bond distance (Å)					
Te-O*	2.204(4)	2.171(7)	2.188(4)	2.180(7)	2.22(2)
	2.259(7)	2.190(6)	2.189(5)	2.183(7)	2.23(1)
		2.198(6)	2.201(4)	2.196(6)	2.24(1)
		2.246(6)	2.254(4)	2.239(6)	2.24(1)
		2.281(6)	2.281(5)	2.266(8)	2.25(1)
		2.301(4)	2.302(3)	2.297(4)	2.27(2)
Average	2.232(4)	2.231(2)	2.236(2)	2.227(3)	2.24(1)
Te-N	2.215(9)	2.189(2)	2.195(3)	2.195(6)	2.18(2)
	2.237(9)	2.203(9)	2.196(5)	2.198(5)	2.21(2)
		2.207(7)	2.204(6)	2.205(8)	2.23(1)
		2.244(1)	2.240(4)	2.243(8)	2.23(2)
		2.252(1)	2.240(6)	2.246(7)	2.25(1)
		2.255(4)	2.253(6)	2.250(7)	2.30(2)
Te-Te*	3.631(1)	3.561(9)	3.5452(5)	3.5706(8)	3.577(2)
	3.664(1)	3.581(6)	3.5882(7)	3.578(1)	3.645(2)
		3.599(5)	3.5976(7)	3.586(1)	3.659(2)
		3.65(6)	3.6644(6)	3.6366(9)	3.679(2)
		3.70(1)	3.6938(7)	3.7031(8)	3.717(3)
		3.730(2)	3.7267(6)	3.735(1)	3.726(2)
Na-O (ligand)		2.30(7)	2.342(8)	2.325(7)	2.36(2)
		3.02(1)	3.08(1)	3.051(8)	3.77(2)
Na-guest		2.31(3)	2.313(8)	2.43(1)	2.37(2)
Na-H_2O		2.27(1)	2.25(1)	2.224(9)	2.24(3)
		2.25(2)	2.421(9)	2.263(7)	
Na-THF					2.33(2)
Bond Angle (º)					
O-N-Te	126.2(6)	125.5(2)	125.7(4)	124.9(5)	124(1)
	126.6(6)	125.5(6)	126.0(3)	125.5(5)	125(1)
		126.5(8)	126.0(3)	125.6(5)	126(1)
		126.6(1)	126.2(3)	125.7(5)	127(1)
		126.7(3)	126.4(4)	125.9(5)	128(1)
		126.7(5)	126.7(4)	126.0(5)	128(1)
Torsion (º)					
Te-N-O-Te	0.3(9)	15.5(8)	14.8(5)	16.0(7)	17(2)
	18.5(8)	16.8(8)	16.4(5)	16.7(7)	20(2)
		20.9(7)	22.7(5)	22.0(7)	23(2)
		24.2(6)	23.7(5)	22.1(7)	24(2)
		24.3(5)	26.0(6)	23.2(7)	24(2)
		27.4(2)	26.1(5)	25.6(8)	26(2)

3.3 Computational Modelling

The relative stability of the dodecamer conformation was contrasted to the reported tetramers and hexamers of iso-tellurazole N-oxides using DFT (ADF, GGA-D3, ZORA, all-electron TZ2P). The models were constructed using **1c** as the building block, and the crystal structure coordinates of the dodecamer were used for calculation with the exclusion of the cyclohexane molecule. The same $(N\text{-}Te\cdots O)_{12}$ backbone was obtained after full optimization and the calculated average d(Te···O) is 2.2808Å, similar to the bond distance observed in $C_6H_{12}\subset\{\mathbf{1a}_{12}\}$. The calculated ΔG, ΔH and ΔS values are shown in Table 3.2. Both the ΔH and ΔS are negative and increase in magnitude with respect to the degree of aggregation. The more negative ΔH is favorable for the dodecamer formation, likely due to the relief of overall ring strain. The Gibbs free energy was used to calculate equilibrium constants in gas phase. These were used to plot the abundance-of-species as a function of concentration for **1c**, $\mathbf{1c}_4$, $\mathbf{1c}_6$ and $\mathbf{1c}_{12}$ (Figure 3.7) at 190K, 298.15K and 340K. Across all temperatures, the cyclic tetramer dominates at lower concentrations, as concentration increase, the concentration of cyclic hexamers increases up till 50%, but it is soon out-competed by the dodecamers. Albeit useful, these diagrams are coarse approximations as solvation is not accounted for.

Table 3.2: Calculated thermodynamic parameters in gas phase at 298.15K.

Equilibrium	ΔH per Te…O interaction (kJ mol^{-1})	ΔS per Te…O interaction (J mol^{-1} K^{-1})
4 1c⇌1c$_4$ (Chair)	-67.6125	-149.22
6 1c⇌1c$_6$	-72.8183	-161.205
12 1c⇌1c$_{12}$	-82.8017	-192.001

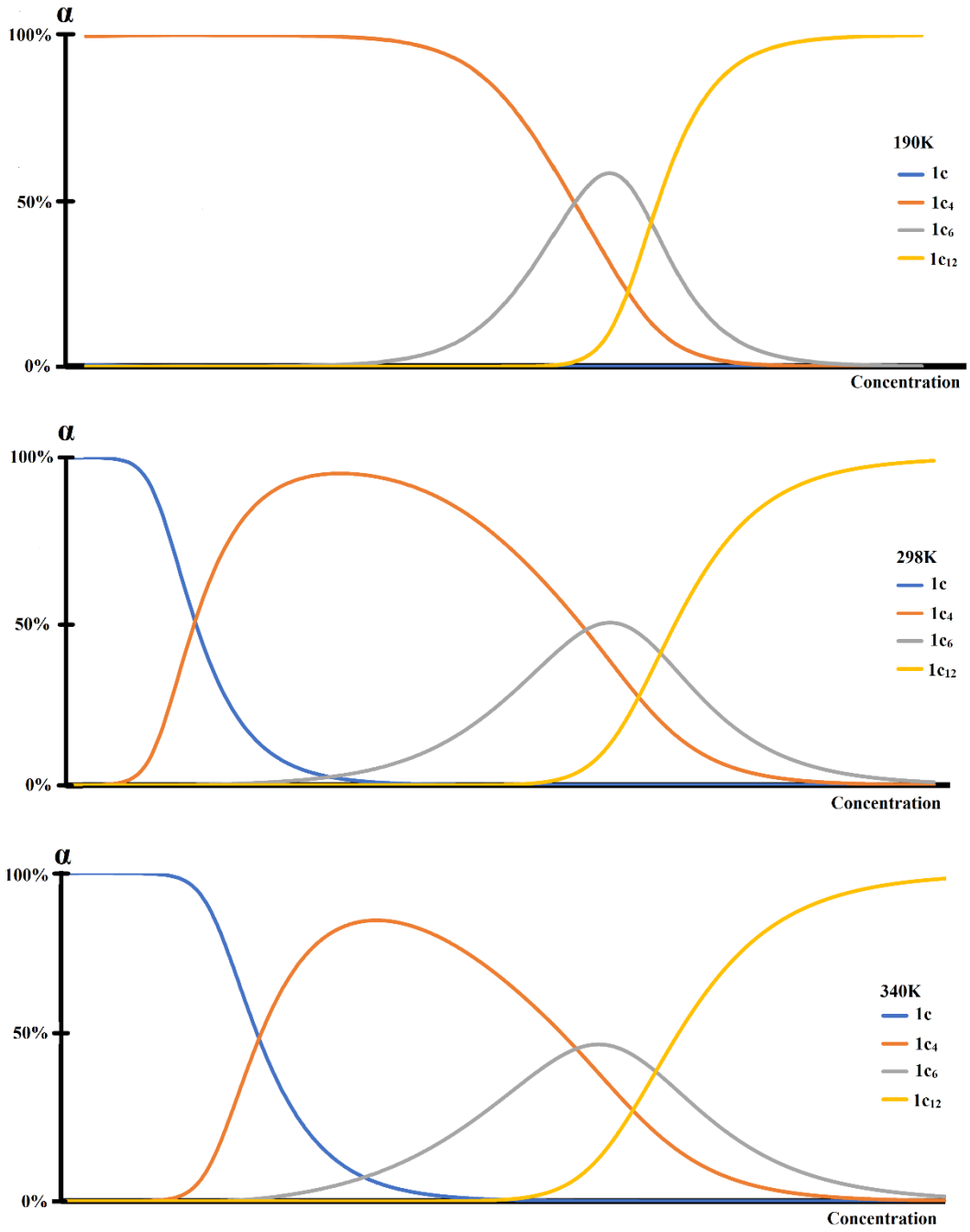

Figure 3.7: The concentration effect on the speciation of iso-tellurazole *N*-oxide at 190 K, 298.15 K and 340 K. The equilibrium constants were calculated in gas phase.

3.4 NMR Spectroscopy

The crystals of $C_6H_{12}\subset\{\mathbf{1a}_{12}\}$ were sparingly soluble in common organic solvents, the resulting spectra had very weak signal to noise ratios. ^{1}H and VT NMR of this compound was attempted from freshly prepared mixtures of the reagents. Stoichiometric mixing of **1a** with cyclohexane (12:1) afforded a spectrum indistinguishable from the combined spectra of the starting materials. The resonance of the guest molecule, showed no significant change from the spectrum of pure cyclohexane in the solvent, which seems unlikely if the molecule were in the electron-rich cavity of a dodecamer.

The spectrum of pure **1a** is characterized by the dynamic $\mathbf{1a}_4$:$\mathbf{1a}_6$ equilibrium in solution.[25] At room temperature, the dominant species is the tetramer and only one set of peaks for the ligand is observed. However, hexamer is more prominent at low temperature and co-exist with tetramer, and the stoichiometry between the two species depends on their concentration. The aromatic resonance of these two species overlap, but the methyl peaks are resolved and can be used to quantify the concentration of each aggregate. To probe the dynamics interactions of **1a** with cyclohexane in solution, VT-NMR of 10:12 ratios of cyclohexane:**1a** were recorded from 298K to 190K with 10K increments. The coalescence of the axial and equatorial proton signals of cyclohexane occurred between 230K-240K, matches to the reference spectra of only cyclohexane. At 190K, the axial and equatorial proton signals of cyclohexane are well separated, and the chemical shift also matches to the reference spectra. Two methyl peaks of **1a** was identified at 190K, indicative of two macrocyclic species co-existing in solution. Their

chemical shift along with the aromatic region pattern matches to the equilibrium between tetramer and hexamer. No additional set of signals was observed in the VT-NMR (Figure 3.8). The polarity of the solvent was also reduced by using CD_2Cl_2 (33% w/w) d-cyclohexane in an attempt to promote aggregation (Figure 3.9). Two set of signals was defined at room temperature, however, the ratio between the two sets of signals at lower temperatures matches the **1a**$_4$:**1a**$_6$ equilibrium.

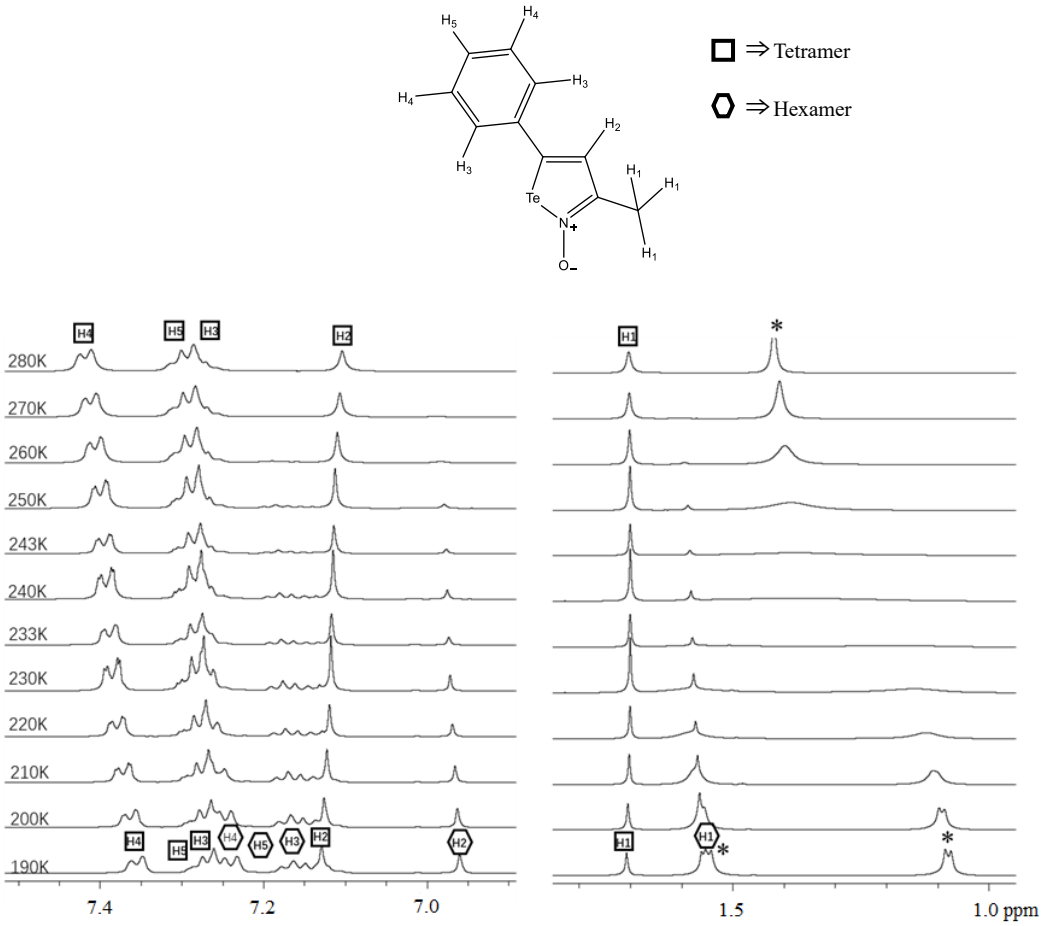

Figure 3.8: VT ^{1}H NMR (500 MHz) of a cyclohexane-**1a** mixture (87mM, 10:12 ratio) in CD_2Cl_2. Assignments of the tetramer (□) and hexamer (⬡) resonances are based on reference 25. * denotes the resonances of cyclohexane.

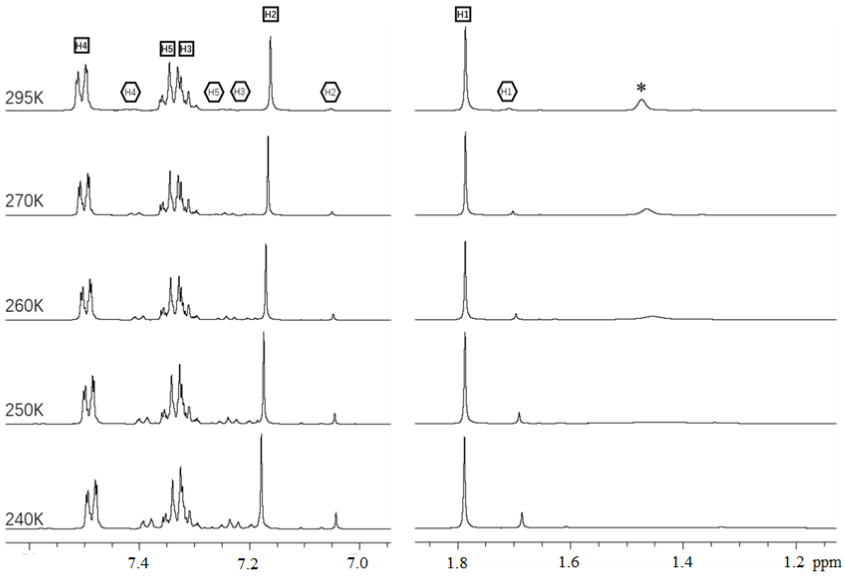

Figure 3.9: VT ^{1}H NMR (500 MHz) of a cyclohexane-**1a** mixture (34mM, 10:12 ratio) in CD_2Cl_2 (33% w/w) d-cyclohexane. Assignments of the tetramer (□) and hexamer (⬡) resonances are based on reference 25. * denotes the resonances of cyclohexane.

Crystals of [1,4-$C_4H_8O_2$⊂{$Na_2(H_2O)_4$(**1b**$_{12}$)}] were collected and redissolved in CD_2Cl_2. The resonance of the proton on position 4 of the heterocycle(H2) at 7.1 ppm has shifted from 7.0 ppm, overlapping with the *ortho*-proton on the phenyl group (Figure 3.10). The $BArF^-$ anion experienced little (<0.01 ppm) chemical shift as expected. The guest molecules show no significant change either. The observed chemical shift in solution matches the chemical shifts of smaller aggregates and do not constitute evidence of dodecamer formation in solution. Therefore, the existence of the dodecamers in solution could not be proved by these experiments, further research is required into suitable conditions that favor the dodecamer.

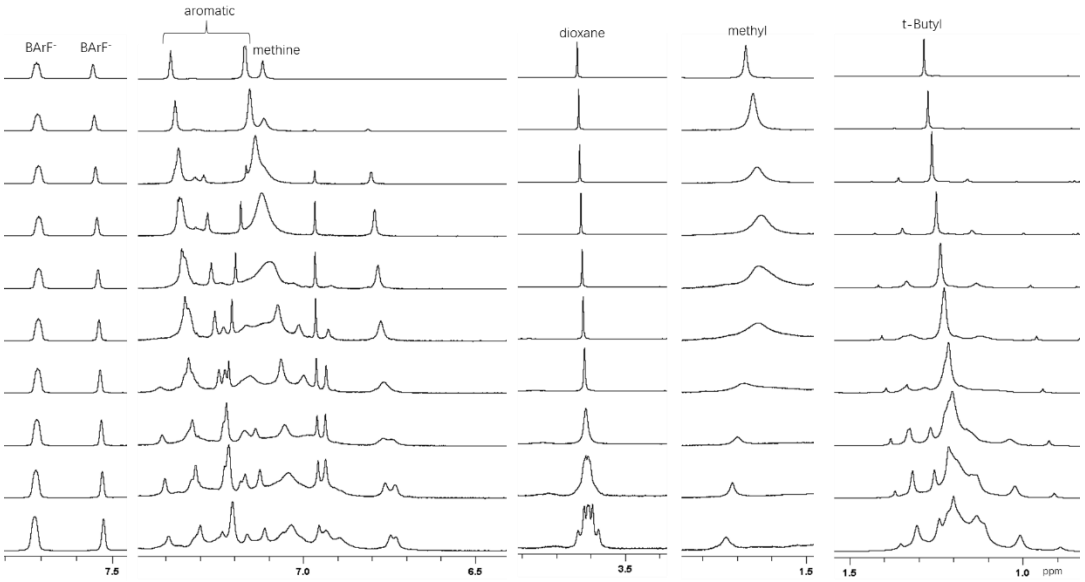

Figure 3.10: VT ^{1}H NMR (500 MHz) of crystalline [1,4-$C_4H_8O_2$⊂{$Na_2(H_2O)_4$(**1b**$_{12}$)}] dissolved in in CD_2Cl_2 to a 14 mM concentration.

3.5 Summary

The crystal structures of the dodecamers, albeit with different functional groups on the ligand and different guest molecules, all share the common $(O\cdots Te\cdots N)_{12}$ backbone. The crystal structure of the cyclohexane complex and thermodynamic parameter analysis indicated that the dodecamers are likely to exist in solution, but finding the conditions to observe their NMR spectra in solution requires further investigations.

Chapter 4: Other complexes of iso-tellurazole *N*-oxides with *s*-block cations

4.1 Introduction

As discussed before, transition metal complexes of **1** have a diverse range of structures. The annular tetramer forms mononuclear complexes with Rh (III), Pd(II), Pt(II), Cu(I); and a dinuclear complex with Au(I). Complexes of the hexamer have been isolated with Ag(I).[29] Albeit some variations are observed between the structures of these species, the metal ions invariably display coordination to tellurium, not to the also electron-rich oxygen. In these complexes, the Te···O distance is shortened as a result of coordination. The oxygen atoms should coordinate hard metal ions; group-1 and 2 cations have much higher affinity towards the oxygen atom than tellurium. Actual data is not available for Te ligands, but a binding study showed that $[K(18\text{-crown-6})]^+$ has a stability constant that is 2-fold and 6-fold higher than those of $[K([18]aneO_5S)]^+$ and $[K([18]aneO_4S_2)]^+$, respectively.[39,40] In the previous chapter, we showed that the dodecamers indeed feature coordination of sodium to the oxygen atom, and the N-Te···O ChB was elongated slightly but not cleaved. However, each Na^+ ion was only coordinated by two oxygen atoms from the dodecamer, and the rest of its coordination sphere was satisfied by H_2O/THF and a guest molecule. In this chapter, we discuss experiments that were conducted in the absence of other small polar molecules. Previous study on the reaction of **1** with mineral acids or BX_3 (X=Ph, F), resulted in O-bonded adduct and enabled Te binding to Lewis bases or even another molecule of **1** (Figure. 4.1). By analogy, binding hard metal ions could lead to similar products.

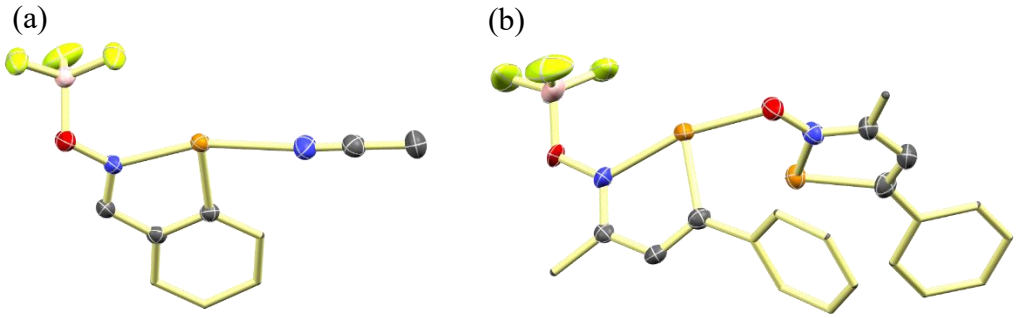

Figure 4.1 Structures of iso-tellurazole N-oxide with Lewis acid and bases. (a) CH_3CN-**1**-BF_3 (b) **1**-**1**-BF_3, from reference 26.

4.2 Result and Discussion

4.2.1 Isolation of [Mg(1a$_6$)](BArF$_{24}$)$_2$ and [Mg(1b$_6$)](BArF$_{24}$)$_2$

Using $[Mg(MeCN)_6](BArF_{24})_2$ and **1a/1b** as starting materials, the Mg(II) complexes, $[Mg(\mathbf{1}_6)](BArF_{24})_2$, were successfully isolated in good yield (Scheme 4.1). Crystallographic parameters are shown in Table 2.1 and selected bond and angles are presented in Table 4.1.

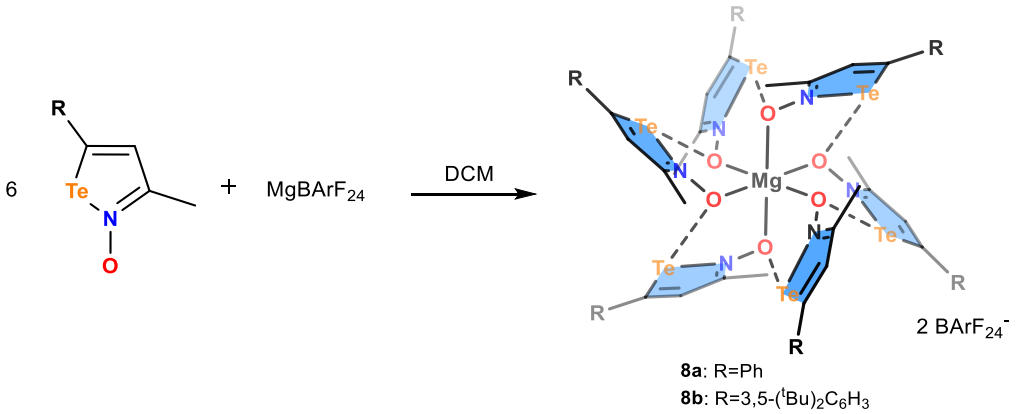

Scheme 4.1: Synthesis overview for Mg(**1**$_6$)(BArF$_{24}$)$_2$.

The Mg(II) center is κ^6O coordinated in a distorted-octahedral geometry (Figure 4.2). The metal ion sits on an inversion centre and there are three ligands in the asymmetric unit. The average d(Mg-O) in [Mg(**1a**$_6$)](BArF$_{24}$)$_2$ is 2.046(2)Å, and cis ∡(O-Mg-O)= 83.5°-96.0°, similar to the structure of the hexa-coordinated Mg(II) with oxides of adenosine 5'-triphosphate, average d(Mg-O)=2.06Å, ∡(O-Mg-O)= 83.4°-97.8°,[41] in contrast to the octahedral κ^6O Mg(II) in $[Mg(H_2O)_6]^{2+}$, which has average d(Mg-O)=2.052(1)Å, ∡(O-Mg-O)= 89.36(6)°-90.64(6)°,[42] and $[Mg(THF)_6]^{2+}$ has average d(Mg-O)=2.085(4)Å, ∡(O-Mg-O)= 88.0(5)°-91.7(4)°.[43] Although the oxygen atoms are bound to the cation, the Te···O distances 2.741(5), 2.787(5) and 2.796(4) Å, are shorter than the sum of van der Waals radii ($\sum r_{vdW}$=3.58Å), but ~0.55Å longer than in **1a**$_{4,6,\infty}$.[25] These Te···O ChBs are formed opposite to the carbon atom, ∡(C-Te···O)= 147.7(2)°- 157.7(2)°. This is the first observed instance of C-Te···O ChBs instead of the usual N-Te···O ChB. The Te-N distance is shortened to 2.07 Å from 2.20 Å, but the Te-C bond distance remains nearly constant. The ligand still constitutes a macrocyclic hexamer, but it is an isomeric structure of the previously-known hexamers.

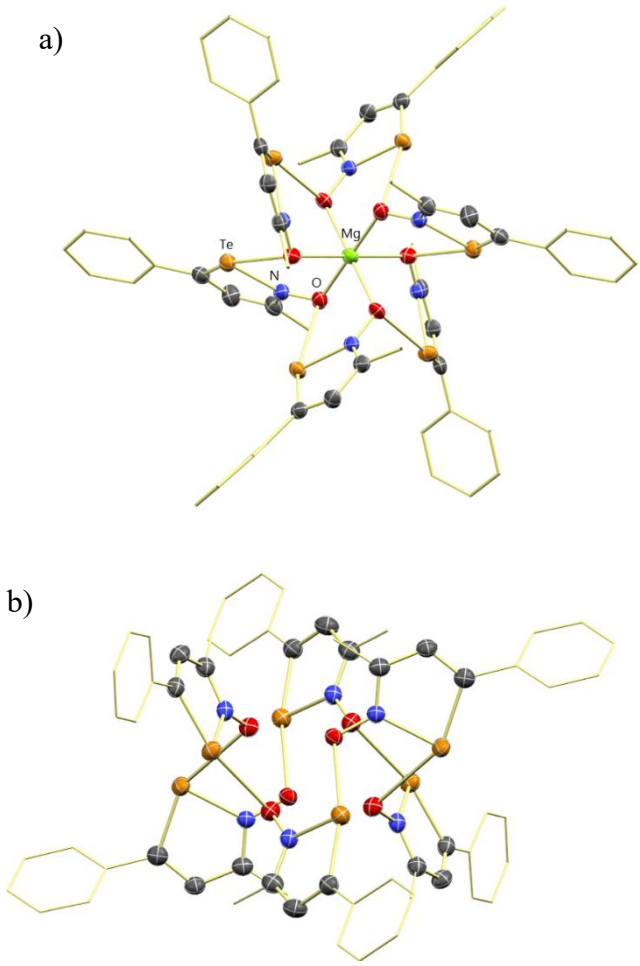

Figure 4.2: Crystal structure of [Mg(**1a**$_6$)](BArF$_{24}$)$_2$. a) Molecular structure of the hexamer. b) The macrocycle with Mg omitted. hydrogen atoms are omitted for clarity. Thermal ellipsoids are shown at 75% probability.

Table 4.1 Selected structural data of the Mg^{2+} complexes.

Crystal	**8**	**9**
	Bond distance (Å)	
Te-O*	2.741(5)	2.770(4)
	2.787(5)	2.776(4)
	2.796(4)	2.783(3)
N-O	1.331(7)	1.339(6)
	1.334(7)	1.349(7)
	1.345(9)	1.349(7)
Te-C	2.073(5)	2.085(5)
	2.078(6)	2.091(7)
	2.083(7)	2.099(5)
Te-N	2.063(7)	2.073(3)
	2.064(7)	2.079(5)
	2.076(6)	2.082(6)
Te-Te*	3.962(2)	4.1366(5)
	4.099(2)	4.2097(7)
	4.228(2)	4.2733(5)
Mg-O	2.039(4)	2.040(3)
	2.048(4)	2.055(3)
	2.052(4)	2.081(3)
	Bond Angle (º)	
C-Te-O	147.7(2)	151.8(2)
	157.5(2)	154.9(2)
	157.7(2)	155.9(2)
O-N-Te	123.6(4)	123.9(3)
	123.8(4)	124.5(4)
	124.4(4)	125.0(3)

The bond distances in [Mg(**1a**$_6$)](BArF$_{24}$)$_2$ are similar to those in **1a**-BF_3. The Te-N bond distance is 2.063(2) Å and Te-C bond distance is 2.081(2) Å. Similar to [Mg(**1a**$_6$)](BArF$_{24}$)$_2$, the Te of **1a**-BF_3 adduct is involved in two ChB interactions (Figure 4.3), the intramolecular d(Te···F) opposite to Te-C is 2.771(3)Å and ∡(C-Te···F)=145.17(1)° is comparable to [Mg(**1a**$_6$)](BArF$_{24}$)$_2$ with avg. d(Te···O)=2.775(3)Å and avg.∡(C-Te···O)=154.3(1)°. The F atom of another molecule of **1a**-BPh_3 act as the ChB acceptor opposite to the Te-N, with d(Te…F)=2.902Å. Similarly, The fluorine

from -CF_3 group of the anion act as the ChB acceptor opposite to Te-N in [Mg(**1a**$_6$)](BArF$_{24}$)$_2$, with Te···F distance as short as 3.301 Å vs Σr_{vdW}=3.53Å.

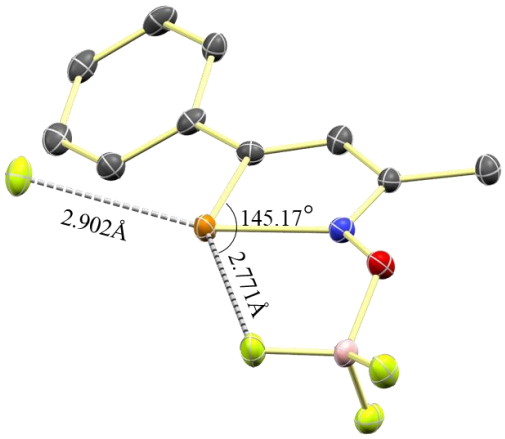

Figure 4.3: Crystal structure of **1a**-BF_3 adduct. Hydrogen atoms are omitted.

4.2.2 Computational Analysis

DFT calculations performed using the ADF DFT package (version 2019.305) were employed to estimate the thermodynamic parameters for the process of aggregation of six **1a** molecules into the new macrocyclic structure and compare them with those of the previously known hexamer. Initial atom coordinates were extracted from the refined crystal structure of [Mg(**1a**$_6$)](BArF$_{24}$)$_2$, excluding the Mg ion, and optimized. For the other structure, the coordinates of **1a**$_6$[25] were also minimized. Upon optimization, the new hexamer geometry was little changed. There was a small contraction of d(Te···O) to 2.6431, 2.6505 Å in two and four ChBs, respectively. The bond angles ∢(C-Te···O)= 155.76, 156.12 and 156.91 ° were similar to those in the crystal structure. The transannular d(O---O) distances (4.4119-4.5245 Å) were larger than in [Mg(**1a**$_6$)](BArF$_{24}$)$_2$ (4.079(8),4.106(7) Å).

The contributions to the electronic energy and the thermodynamic parameters at 298.15 K are shown in Table 4.2. As calculated by ADF, the total bonding energy (E_{TB}) of includes several contributions:[43]

$$E_{TB} = E_{Pauli} + E_{elstat} + E_{orbital} + E_{disp}$$

The Pauli energy (E_{Pauli}) is results from the interaction of the electrons in full shells and consequently is repulsive. The electrostatic contribution (E_{elstat}) results from the interaction between asymmetric distributions of charge. Both E_{Pauli} and E_{elstat} are calculated with frozen orbitals. Their combination was termed the steric interaction (E_{steric}) by Ziegler and Rauk,[38] but this name can be confusing as it often used as synonymous of the Pauli interaction only. Relaxation of the electron density by mixing of wave functions gives the orbital interaction ($E_{orbital}$). The original formalism has been revised to include a dispersion correction (E_{disp}). In modeling the process of aggregation, the changes to these quantities represent the contributions to the supramolecular interaction energy. In the case of the assembly of the hexamers from their constituting molecular building blocks, this is the binding energy from six Te···O ChBs:

$$\Delta E_{Aggregation} = \Delta E_{Pauli} + \Delta E_{elstat} + \Delta E_{orbital} + \Delta E_{disp} = 6\ \Delta E_{Te\cdots O}$$

These terms are strictly electronic in origin. Calculation of the thermodynamic parameters requires the calculation of the normal vibrational modes of the system. The nuclear internal energy is calculated from the Zero Point Energy (ZPE), 3/2 k_BT for each translational and rotational degree of freedom and a correction term from the vibrational partition function. For a nonlinear molecule with n atoms:

$$\frac{E_{nuclear}}{N_A} = ZPE + 6\,\frac{3}{2}\,k_B + \sum_{j}^{3n-6}\left(\frac{h\vartheta_j}{2} + \frac{h\vartheta_j}{e^{h\vartheta_j/(k_B T)} - 1}\right) - D$$

Where D is the dissociation energy. The total internal energy (U) is the sum of the electronic and nuclear components:

$$U = E_{TB} + E_{nuclear}$$

From which the molar enthalpy and Gibbs free energy are:

$$H = U + pV$$

$$G = H + TS$$

Table: 4.2 Energy decomposition analysis for the two different hexamer geometries. All values in kJ mol^{-1} unless otherwise noted. All terms are divided by 6 to scale the effects to one Te···O ChB.

	ChBs in **1a$_6$**	
Contribution	**(N-Te···O)**	**(C-Te···O)**
$\Delta E_{Pauli}/6$	-283.34	34.28
$\Delta E_{elst}/6$	-9.04	-54.01
$\Delta E_{steric}/6$	-292.38	-19.73
$\Delta E_{orbital}/6$	244.73	5.87
$\Delta E_{disp}/6$	-29.66	-26.18
$\Delta E_{Aggregation}/6$	-77.31	-40.05
$\Delta ZPE/6$	2.46	1.73
$\Delta E_{nuclear}/6$	3.41	2.76
$\Delta U/6$	-73.90	-37.29
$\Delta H/6$	-75.97	-39.35
ΔS(J mol^{-1} K^{-1})/6	-190.16	-183.20
ΔG(298.15 K)/6	-19.28	15.27

Based on the overall electronic contributions ($\Delta E_{Aggregation}$) alone, both macrocyclic hexamers would be stable. However, the thermodynamic parameters indicate that only the previously observed hexamer would be stable at 298.15 K. The arrangement as

observed around Mg(II) could not exist without the metal ion. The entropic contributions are nearly identical; therefore, the main difference is due to the enthalpy of aggregation. In other words, C-Te···O ChBs are not strong enough to stabilize the aggregate at room temperature.

Attempts to crystallize complexes with the other alkaline-earth cations did not yield crystals of quality appropriate for crystallographic determination, the C-Te···O ChB competes with the other more favorable chalcogen bonding interaction, and with the increase in size of the heavier elements down the group, the complex is stretched. This changes result in further C-Te···O ChBs. Therefore, the novel hexamer geometry was used as a basis for DFT calculation for all group 2 metals ions. The calculated Mg complex shows geometry similar to the experimental one, the average d(Te···O) is slightly increased to 2.8227Å, and the average ∢(C-Te···O) is 153.99° (Figure 4.4). The calculated Be structure has a similar geometry. However, significant distortions of the octahedral structure are observed for the heavier group-2 elements. The metal ions sit out of the plane formed by the four equatorial oxygen atoms and approach the octahedron face defined by two equatorial- and one axial- oxygen atoms. The Ba structure has the metal ion in the plane of the triangular face, with all six ligands coordinated to its top hemisphere and bottom hemisphere exposed. Interestingly, the C-Te···O bonding interaction was conserved in all the calculated structures despite such structural changes. The list of d(Te···O) and ∢(C-Te···O) are shown in Table 4.3.

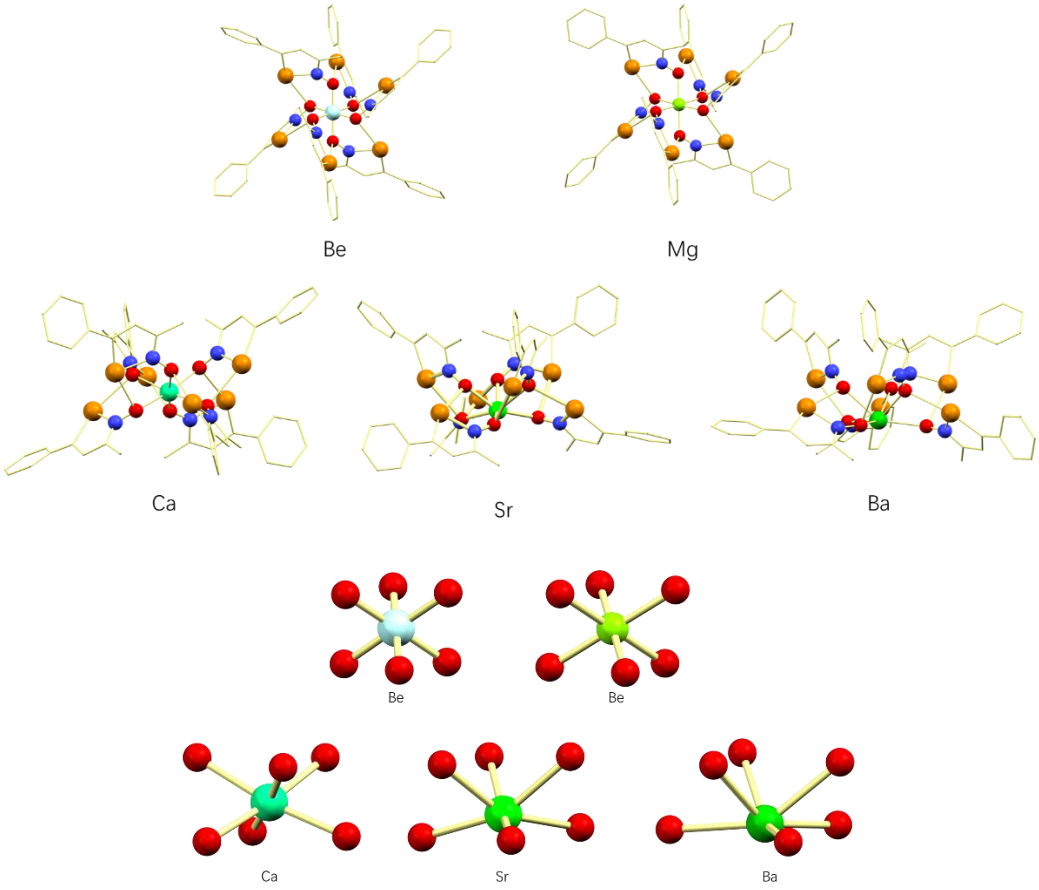

Figure 4.4: a) Calculated geometries of group 2 elements. Hydrogen atoms are omitted for clarity. b) The metal-centre coordination environment of group 2 elements.

Table 4.3: Calculated ChB distances and angles for all group 2 elements.

	Avg. d(Te···O) Å	**Avg. ∡(C-Te···O) °**
Be	2.7920	150.6433
Mg	2.8227	153.9900
Ca	2.8174	158.1833
Sr	2.8725	158.1933
Ba	2.8765	158.2367

4.2.3 Isolation of the $[Na_4(\mathbf{1a}_4)_3](BArF_{24})_4$ tris-tetramer

The reaction of $Na(BArF_{24})$ with **1a** afforded $[Na_4(\mathbf{1a}_4)_3](BArF_{24})_4$. The isolated single crystal was a very thin plate which complicated the refinement of this structure. Attempts to induce crystallization in different conditions did not give better crystals. The crystal structure features three macrocyclic tetramers in a twist-boat conformation, interconnected by a total of four Na^+ ions (Figure 4.5). The twist-boat conformation has been observed with the benzo-1,2-tellurazole 2-oxides.[44] The former geometry has significant smaller trans-annular Te-Te distance as a result of bending the $(N\text{-}Te\cdots O)_4$ ring. Each tetramer in this structure has two unique trans-annular Te-Te distances. The tetramer coordinated by both Na1 and Na2 has trans d(Te-Te)=5.246(1) and 5.367(7) Å, whereas the tetramer coordinated by only Na1 has trans d(Te-Te)=5.286(5) and 5.392(3) Å, and the tetramer coordinated only to Na2 has trans d(Te-Te)=5.292(7) and 5.396(8) Å. These distances are all shorter than in the chair $\mathbf{1a}_4$, trans d(Te-Te)= 5.3044(3) and 5.5897(4) Å, but the boat conformation adopted by the $[\mathbf{1a}_4]C_{60}$ adduct has a shorter trans d(Te-Te)= 5.0530(7) and a longer d(Te-Te)=5.4210(8) Å.[25] Each tetramer has four distinct Te···O distances, spanning from 2.206(8)- 2.387(7) Å with average equals to 2.307(6) Å, significantly higher than the average d(Te···O) observed for $\mathbf{1a}_{4,6,12}$ and the Na-dodecamer complexes.

Four Na^+ ions was found for each tris-tetramer, also confirmed by the four bystander disordered anions. Na1 and Na2 are coordinated by two tetramers, while Na3 and Na4 are coordinated by three tetramers. The axis formed by Na1-Na2 is

perpendicular to the axis formed by Na3-Na4. The electron density in the central cavity could not be refined but is likely to be occupied by disordered dichloromethane. Both Na1 and Na2 are κ^2O and $[\eta^5(C_6H_5)]_2$, d(Na-O) is 2.272(4)- 2.304(6) Å. Na3 and Na4 are coordinated by three oxygens, each from a different tetramer, but Na3 has d(Na-O) = 2.3046, 2.3082 and 2.3092 Å, and Na4 extends more into the cavity and d(Na-O) = 2.6823, 2.8293 and 2.8491 Å. The axial Na^+ ions link the three macrocycles into the cage-like structure.

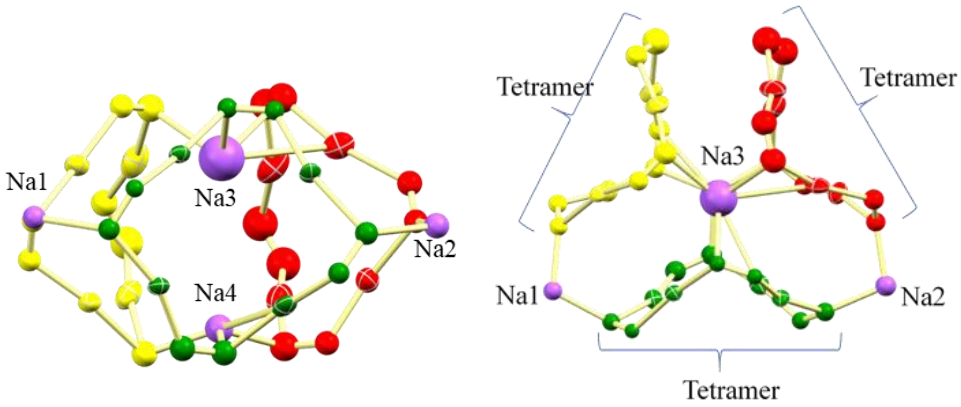

Figure 4.5: Crystal structure of $[Na_4(\mathbf{1a}_4)_3]^{4+}$. Green, yellow, and red colours identify individual tetramers. Carbon and hydrogen atoms are omitted for clarity, thermal ellipsoids are at 75% probability. Views of the structure perpendicular (left) and along (right) the Na3-Na4 axis.

Coordination of the oxygen atom to Na did not disrupt the chalcogen bonding of the macrocyclic assembly of **1**, instead, through coordination of the oxygen atoms, three tetramers are recruited as building blocks to form the cage-like structure.

Crystal structures of the dodecamers and tris-tetramers differ in their (N-Te···O) backbones and the number of sodium atoms but, despite these differences, a closer

analysis of the tris-tetramer (N-Te···O) linkage reveals a possible route to the dodecamer. Enabled by the reversible nature of the ChBs in the aggregates of **1**, a mechanism for the conversion of the tris-tetramer to the dodecamer is proposed in Figure 4.6. Upon inclusion of a suitable guest, opening of one ChB in each of the cyclic tetramer would allow neighbouring tetramers to link into a single macrocycle once ChBs are reconstituted. The Na^+ ions in the polar positions would remain coordinated to the dodecamer, but the equatorial Na^+ would be released in the process.

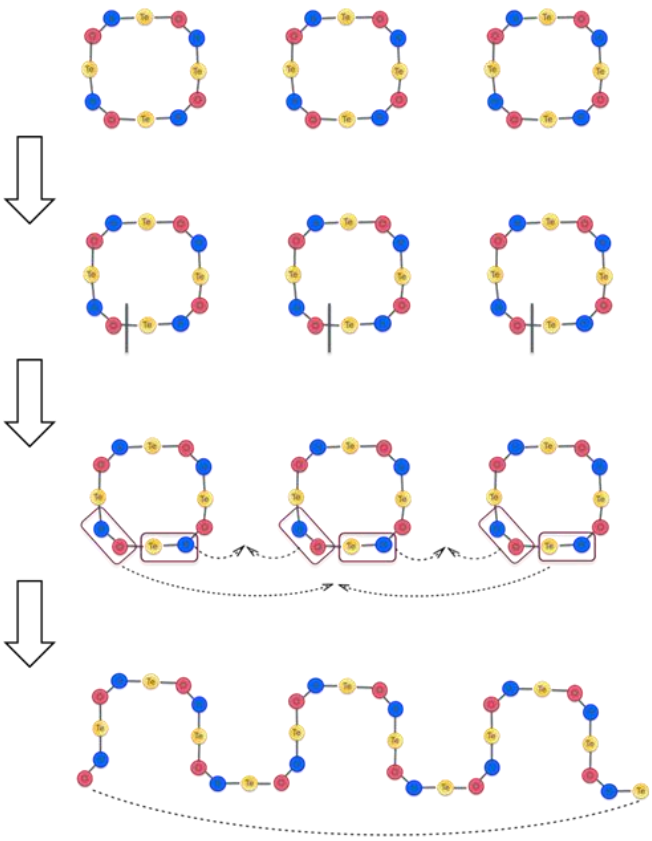

Figure 4.6: Proposed ChB rearrangement to form a dodecamer from three tetramers of **1**. The dashed arrows represent the change in the direction of the ligand, to form ChB with neighbouring tetramers.

4.2.4 Isolation of [K(1a$_4$)](BArF$_{20}$), a 1D coordination polymer

$KBArF_{24}$ is poorly soluble, instead a reaction was attempted with $KBArF_{20}$. Liquid-liquid diffusion with Fluorobenzene/n-Hexane allowed slow growth of crystals of composition [K(**1a$_4$**)](BArF$_{20}$) (Scheme 4.2), prolonged mixing led to precipitation of the pure product out of solution. The tetramer and $KBArF_{20}$ are in 1:1 stoichiometry.

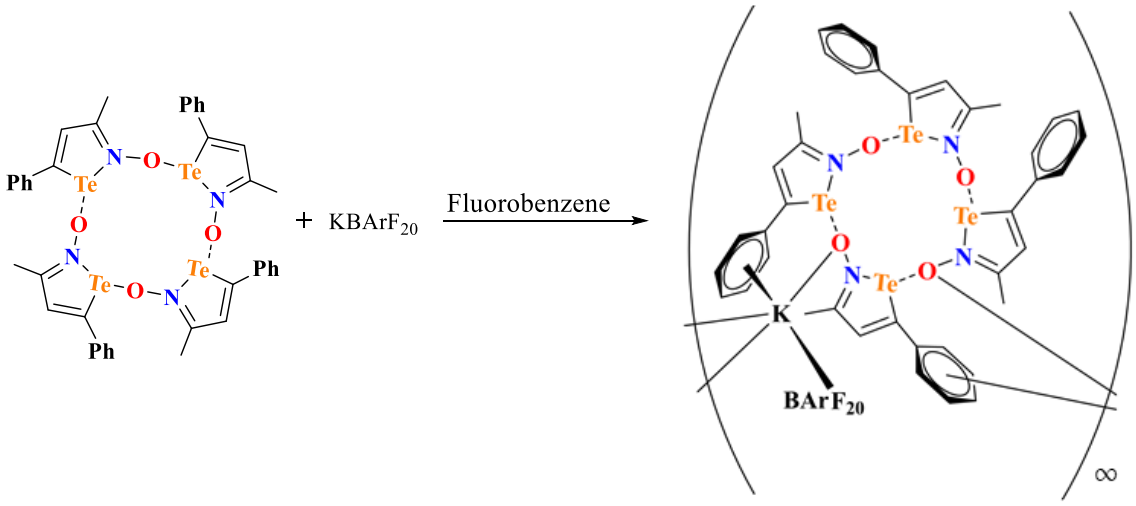

Scheme 4.2: Synthesis of [K(**1a$_4$**)](BArF$_{20}$). F atoms belong to the anions.

The crystal structure of this product features tetramers in boat conformation linked by K^+ ions in a coordination polymer. The tetramer is κ^2O and $[\eta^5(C_5H_6)]_2$ coordinated to K^+, which also displays a weak interaction with the C_6F_5 group of the anion (Figure 4.7). The coordination geometry of K is similar to the K complexes coordinated by two phenyl groups and two neutral oxygen atoms (Figure 4.8).[45,46] Bond distances d(K-O)= 2.68(1) and 2.70(1)Å, d(K-C)= 3.17(2)- 3.38(2)Å and d(K-F)= 2.69(1) Å are similar to reported examples, but ∡(O-K-O) is 160.4(4)° in contrast to 128.7(3)° in **11**,[46] and the bond angle is further decreased to 78.73° in **12**.[45]

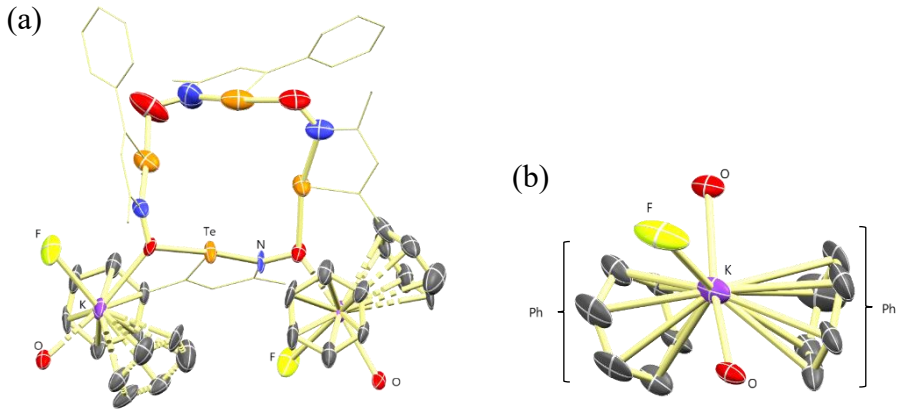

Figure 4.7: Crystal structure of [K(**1a**$_4$)](BArF$_{20}$). a) Showing the interaction of tetramer with K^+ with thermal ellipsoid at 75% probability. Hydrogen atoms are omitted for clarity. b) View of the coordination environment of K.

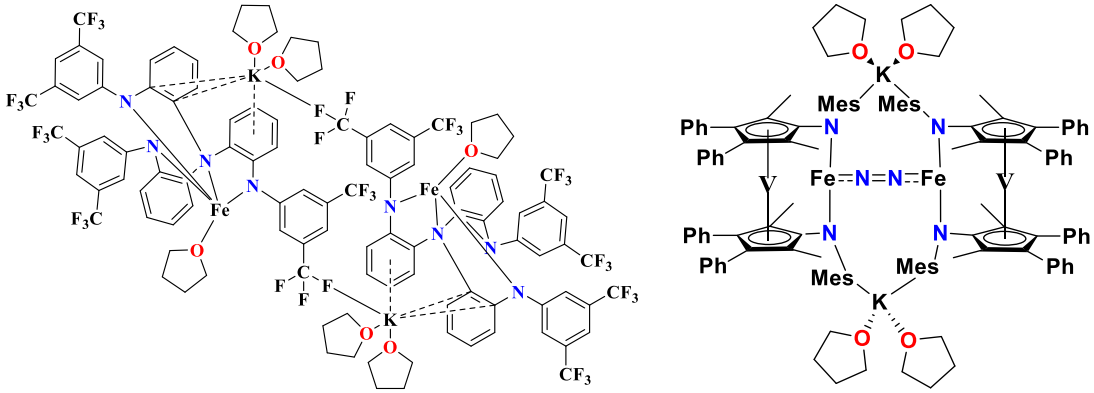

Figure 4.8. Lewis structure for a dimer of [K(THF)$_2$][((3,5-(CF$_3$)$_2$Ph)-NH-(2-C$_6$H$_4$))$_3$N)Fe^{II}-THF] and [K(THF)$_2$]$_2${(Cp′NMes)$_2$VFe}$_2$(μ-N$_2$).

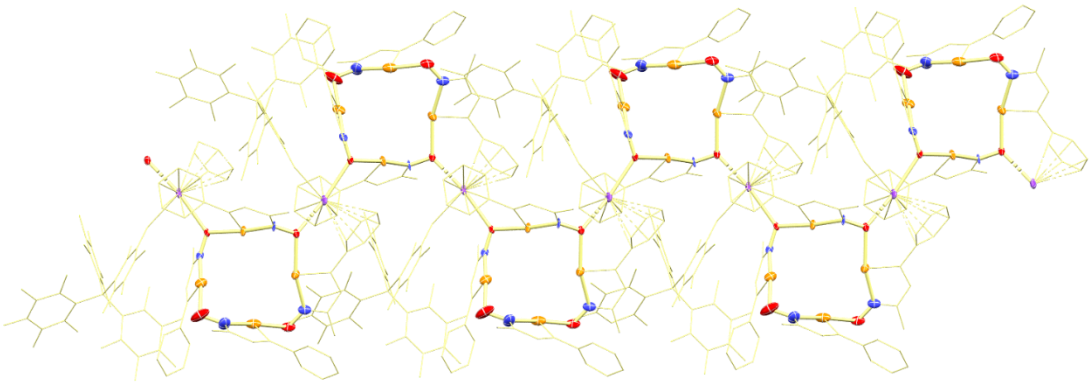

Figure 4.9: Portion of the polymeric chain in [K(**1a**$_4$)](BArF$_{20}$). The anion sits in between the space of two adjacent tetramers, with one of its C_6F_5 group coordinated to K. Hydrogen atoms are omitted for clarity, the thermal ellipsoids are shown at 75% probability.

The ranges of Te···O (2.17(2)-2.36(1)Å), d(Te-N) (2.16(2)-2.21(2)Å) distances, and ∡ (C-Te···O)= (163.4(5)-168.1(6)°) in the tetramer are comparable to those in [Na$_4$(**1a**$_4$)$_3$](BArF$_{24}$)$_4$, but unlike the tris-tetramer with Na, the structure with K features a coordination polymer (Figure 4.9).

Attempts to isolate heavier alkali metal derivatives (Rb^+, Cs^+) have been unsuccessful, higher coordination numbers are expected for these large sized ions. Further research with the heavier analogues is needed to elucidate the interaction of those metal ions with **1**. The increase in ionic size is likely to favour new geometric arrangements.

The group 1 cations together with the use of only weakly coordinating anions and avoiding the use of donor solvents, is coordinated by the oxygen and phenyl groups of

1. Although only tetramer complexes were isolated in those complexes, these cations should not be selective towards tetramers or hexamers, especially in the polymeric K complex, which only interacts with two adjacent ligands. As previously demonstrated by Ho *et al.*, the dominating species at room temperature in solutions of **1a-b** is the tetramer, whereas at 190 K, the equilibrium is shifted towards hexamer.[25] The hexamer geometry with larger ring size and less ring strain could be a better fit for heavier analogues, such as Cs^+. The relation between group-1 elements complex with hexamers should be investigated in future experiments.

4.3 Summary

The annular structure of the aggregates of **1** was not affected by the coordination of oxygen to group-1 and 2 cations. With Mg^{2+}, **1** satisfies the coordination sphere of the central Mg while forming C-Te···O ChBs and a new hexameric arrangement. The tris-tetramer structure isolated with Na and the polymeric structure isolated with K, both display coordination external to the macrocycle. Trivalent lanthanides are strongly oxophilic and favour large coordination numbers, thus they should be the next in the list of cations to bind to **1**. Derivatives of **1** with R=alkyl should also be investigated as they lack the aromatic groups that appear to stabilize the Group-1 complexes in this chapter. A systematic study with other *s*- and *f*-block elements will help the understanding and eventually manipulation of these supramolecular building blocks.

Chapter 5. Conclusion and outlook

5.1 Conclusion

The results of the research described in this thesis identified new aggregates of iso-tellurazole *N*-oxide.

Crystals structures of the products isolated with Group 1 cations (Na^+ and K^+) did show coordination of the metal to oxygen, but are all structurally different from one another. Simply adding small polar molecules led to different coordination modes in the dodecamers or the tris-tetramer complex with Na^+, whereas a coordination polymer was isolated with K^+. Albeit the structural differences, metal ions in tris-tetramer and coordination polymer share similar coordination environments. Attempts to observe dodecamer formation in solution by NMR was unsuccessful.

However, in the case of Group 2 cation, Mg^{2+}, the metal ion is coordinated by six molecules of iso-tellurazole *N*-oxide, which completely disrupted the N-Te···O ChB backbone. These small molecules in turn formed the weaker C-Te···O ChBs and a new macrocycle, which might not stable enough to exist on its own. Computational studies suggest heavier Group 2 cations would prefer high coordination numbers, and the macrocycle formed by C-Te···O ChBs is very flexible.

While most of the products were structurally authenticated by X-ray diffraction, problems such as slow crystal growth, poor crystal quality and disorder, greatly complicated their characterization.

5.2 Suggestions of Future Work

The investigations with Na^+ and K^+ showed the N-Te···O ChB is not broken upon coordination to the oxygen, and that two coordination modes were observed with Group 1 cations. It would be very interesting to examine the coordination of the heavier Group-1 cations with **1** alone or with ancillary ligands. The hexamer is not the limit of size of the supramolecular aggregates of **1**. Aggregation numbers larger than 12 might be possible in suitable conditions. Computational studies of the Group 2 cations suggest that the C-Te···O ChBs in a complex are resilient to structural changes. Therefore, large metal ions such as Ba^{2+} could lead to yet new structures. The same concept can be applied complexes of *f*-block elements.

Moreover, recent discoveries had revealed the reduction of 2,1,3-benzotelluradiazole affordes the unsymmetric trimeric dianion $[L_3]^{2-}$ (Figure 5.1),[47] in which the unpaired electrons are delocalized through the ChBs. The Te-N bond distance in the trimer is longer than in individual molecules. However, the Te···N distances are notably shorter in comparison to structures in the literature. The structure is stabilized by coordination to potassium ions on the two terminal nitrogen atoms. These findings and DFT calculations suggest that two-electron reduction could lead to a neutral [Mg(**1**$_6$)], in which two unpaired electrons would be delocalized over the hexamer due to its S_6 symmetry.

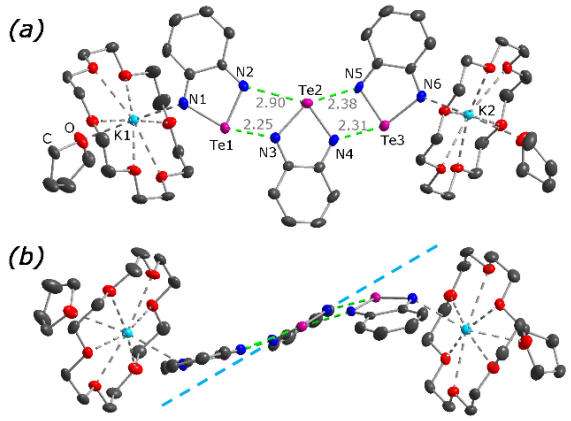

Figure 5.1: The crystal structure of the reduced 2,1,3-benzotelluradiazole trimer. (a) depicts the four different chalcogen bonding distances. (b) displays the distortion of the trimer from linearity. Reproduced from reference 47.

References:

(1) Lindoy, C. L. F. *J. Coord. Chem.* **1990**, *21* (1), 87-87.

(2) Frija, L. M. T.; Pombeiro, A. J. L.; Kopylovich, M. N. *Coord. Chem. Rev.* **2016**, *308*, 32–55.

(3) Rowan, S. J.; Cantrill, S. J.; Cousins, G. R. L.; Sanders, J. K. M.; Stoddart, J. F. *Angew. Chem. Int. Ed.* **2002**, *41* (6), 898-952.

(4) Rezaeivala, M.; Keypour, H. *Coord. Chem. Rev.* **2014**, *280*, 203–253.

(5) Rodewald, M.; Rautiainen, J. M.; Niksch, T.; Görls, H.; Oilunkaniemi, R.; Weigand, W.; Laitinen, R. S. *Chem. Eur. J.* **2020**, *26* (61), 13806–13818.

(6) Fujihara, H.; Ninoi, T.; Akaishi, R.; Erata, T.; Furukawa, N. *Tetrahedron Lett.* **1991**, *32* (35), 4537–4540.

(7) Takaguchi, Y.; Horn, E.; Furukawa, N. *Organometallics* **1996**, *15* (24), 5112–5115.

(8) Hesford, M. J.; Levason, W.; Matthews, M. L.; Reid, G. *Dalton Trans.* **2003**, *3* (14), 2852–2858.

(9) Panda, A.; Panda, S.; Srivastava, K.; Singh, H. B. *Inorg. Chim. Acta* **2011**, *372* (1), 17–31.

(10) Cavallo, G.; Metrangolo, P.; Milani, R.; Pilati, T.; Priimagi, A.; Resnati, G.; Terraneo, G. *Chem. Rev.* **2016**, *116* (4), 2478–2601.

(11) Burchell, T. J.; Eisler, D. J.; Puddephatt, R. J. *Inorg. Chem.* **2004**, *43* (18), 5550–5557.

(12) Stang, P. J.; Olenyuk, B. *Acc. Chem. Res.* **1997**, *30* (12), 502–518.

(13) Gong, B. *J. Am. Chem. Soc.* **2005**, *127* (10), 3643–3644.

(14) Gleiter, R.; Werz, D. B. *Chem. Lett.* **2005**, *34* (2), 126–131.

(15) Lari, A.; Gleiter, R.; Rominger, F. *Eur. J. Org. Chem.* **2009**, *2009* (14) , 2267–2274.

(16) Werz, D. B.; Staeb, T. H.; Benisch, C.; Rausch, B. J.; Rominger, F.; Gleiter, R. *Org. Lett.* **2002**, *4* (3), 339–342.

(17) Garrett, G. E.; Gibson, G. L.; Straus, R. N.; Seferos, D. S.; Taylor, M. S. *J. Am. Chem. Soc.* **2015**, *137* (12), 4126–4133.

(18) Cozzolino, A. F.; Whitfield, P. S.; Vargas-Baca, I. *J. Am. Chem. Soc.* **2010**, *132* (48), 17265–17270.

(19) Suturina, E. A.; Semenov, N. A.; Lonchakov, A. V.; Bagryanskaya, I. Y.; Gatilov, Y. V.; Irtegova, I. G.; Vasilieva, N. V.; Lork, E.; Mews, R.; Gritsan, N. P.; Zibarev, A. V. *J. Phys. Chem. A* **2011**, *115* (18), 4851–4860.

(20) Semenov, N. A.; Lonchakov, A. V.; Pushkarevsky, N. A.; Suturina, E. A.; Korolev, V. V.; Lork, E.; Vasiliev, V. G.; Konchenko, S. N.; Beckmann, J.; Gritsan, N. P.; Zibarev, A. V. *Organometallics* **2014**, *33* (16), 4302–4314.

(21) Cozzolino, A. F.; Dimopoulos-Italiano, G.; Lee, L. M.; Vargas-Baca, I. *Eur. J. Inorg. Chem.* **2013**, *2013* (15), 2751–2756.

(22) Cozzolino, A. F.; Vargas-Baca, I. *J. Organomet. Chem.* **2007**, *692* (13), 2654–2657.

(23) Kremer, A.; Fermi, A.; Biot, N.; Wouters, J.; Bonifazi, D. *Chem. Eur. J.* **2016**, *22* (16), 5665–5675.

(24) Garrett, G. E.; Carrera, E. I.; Seferos, D. S.; Taylor, M. S. *Chem. Commun.* **2016**, *52* (64), 9881–9884.

(25) Ho, P. C.; Szydlowski, P.; Sinclair, J.; Elder, P. J. W.; Kübel, J.; Gendy, C.; Lee, L. M.; Jenkins, H.; Britten, J. F.; Morim, D. R.; Vargas Baca, I. *Nat. Commun.* 2016, *7*, 11299.

(26) Ho, P. C.; Lee, L. M.; Jenkins, H.; Britten, J. F.; Vargas-Baca, I. *Can. J. Chem.* **2016**, *94* (5), 453–457.

(27) Ho, P. C.; Jenkins, H. A.; Britten, J. F.; Vargas-Baca, I. *Faraday Discuss.* **2017**, *203*, 187–199.

(28) Ho, P. C.; Bui, R.; Cevallos, A.; Sequeira, S.; Britten, J. F.; Vargas-Baca, I. *Dalton Trans.* **2019**, *48* (15), 4879–4886.

(29) Wang, J.; Ho, P. C.; Britten, J. F.; Tomassetti, V.; Vargas-Baca, I. *New J. Chem.* **2019**, *43* (32), 12601–12608.

(30) Martínez-Martínez, A. J.; Weller, A. S. *Dalton Trans.* **2019**, *48* (11), 3551–3554.

(31) Shyshov, O.; Brachvogel, R.; Bachmann, T.; Srikantharajah, R.; Segets, D.; Hampel, F.; Puchta, R.; Delius, M. Von. *Angew. Chem. Int. Ed.* **2017**, *56* (3), 776-781.

(32) Carreras, L.; Rovira, L.; Vaquero, M.; Mon, I.; Martin, E.; Benet-Buchholz, J.; Vidal-Ferran, A. *RSC Adv.* **2017**, *7* (52), 32833–32841.

(33) Levason, W.; Pugh, D.; Purkis, J. M.; Reid, G. *Dalton Trans.* **2016**, *2*, 7900–7911.

(34) Sheldrick, G. M. *Acta Crystallogr. Sect. C Struct. Chem.* **2015**, *71*(1), 3–8.

(35) MacRae, C. F.; Sovago, I.; Cottrell, S. J.; Galek, P. T. A.; McCabe, P.; Pidcock, E.; Platings, M.; Shields, G. P.; Stevens, J. S.; Towler, M.; Wood, P. A. *J. Appl. Crystallogr.* **2020**, *53*, 226–235.

(36) Perdew, J. P.; Burke, K.; Ernzerhof, M. *Phys. Rev. Lett.* **1997**, *78* (7), 1396–1396.

(37) Van Lenthe, E.; Snijders, J. G.; Baerends, E. J. *J. Chem. Phys.* **1996**, *105* (15), 6505–6516.

(38) Ziegler, T.; Rauk, A. *Inorg. Chem.* **1979**, *18* (7), 1755-1759

(39) Frensdorff, H. K. *J. Am. Chem. Soc.* **1971**, *93* (3), 600–606.

(40) Lamb, J. D.; Izatt, R. M.; Swain, C. S.; Christensen, J. J. *J. Am. Chem. Soc.* **1980**, *102* (2), 475–479.

(41) Cini, R.; Burla, M. C.; Nunzi, A.; Polidori, G. P.; Zanazzi, P. F. *J. Chem. Soc. Dalton Trans.* **1984**, No. 11, 2467–2476.

(42) Smith, G.; Wermuth, U. D.; Williams, M. L. *Acta Cryst. E* **2011**, *67* (9), 0–7.

(43) Doyle, L. R.; Wooles, A. J.; Liddle, S. T. *Angew. Chem. Int. Ed.* **2019**, *58* (20), 6674–6677.

(44) Ho, P. C.; Rafique, J.; Lee, J.; Lee, L. M.; Jenkins, H. A.; Britten, J. F.; Braga, A. L.; Vargas-Baca, I. *Dalton Trans.* **2017**, *46* (20), 6570–6579.

(45) Hatanaka, T.; Kusunose, H.; Kawaguchi, H.; Funahashi, Y. *Eur. J. Inorg. Chem.*

2020, *2020* (15–16), 1449–1455.

(46) Paraskevopoulou, P.; Ai, L.; Wang, Q.; Pinnapareddy, D.; Acharyya, R.; Dinda, R.; Das, P.; Çelenligil-Çetin, R.; Floros, G.; Sanakis, Y.; Choudhury, A.; Rath, N. P.; Stavropoulos, P. *Inorg. Chem.* **2010**, *49* (1), 108–122.

(47) Puskarevsky, N. A.; Smolentsev, A. I.; Dmitriev, A. A.; Vargas-Baca, I.; Gritsan, N. P.; Zibarev, A. V. *Chem. Comm.* **2020**, *56*, 1113-1116.